2013-04-12

Analysis of Long-term Borehole and Seafloor Pressure Data Recorded by the Subseafloor Observatories in Middle Valley, Northern Juan de Fuca Ridge

Katherine E. Inderbitzen
University of Miami, inderbitzen@gmail.com

UNIVERSITY OF MIAMI

ANALYSIS OF LONG-TERM BOREHOLE AND SEAFLOOR PRESSURE DATA RECORDED BY THE SUBSEAFLOOR OBSERVATORIES IN MIDDLE VALLEY, NORTHERN JUAN DE FUCA RIDGE

By

Katherine E. Inderbitzen

A DISSERTATION

Submitted to the Faculty
of the University of Miami
in partial fulfillment of the requirements for
the degree of Doctor of Philosophy

Coral Gables, Florida

May 2013

UNIVERSITY OF MIAMI

A dissertation submitted in partial fulfillment of
the requirements for the degree of
Doctor of Philosophy

ANALYSIS OF LONG-TERM BOREHOLE AND SEAFLOOR PRESSURE DATA RECORDED BY THE SUBSEAFLOOR OBSERVATORIES IN MIDDLE VALLEY, NORTHERN JUAN DE FUCA RIDGE

Katherine E. Inderbitzen

Approved:

_____ Keir Becker, Ph.D. Professor of Marine Geology & Geophysics	_____ M. Brian Blake, Ph.D. Dean of the Graduate School
_____ Timothy Dixon, Ph.D. Professor of Marine Geology & Geophysics	_____ Guoqing Lin, Ph.D. Professor of Marine Geology & Geophysics

_____
Earl Davis, Ph.D.
Research Scientist
Pacific Geoscience Centre, Geological Survey of Canada

INDERBITZEN, KATHERINE E. (Ph.D., Marine Geology and Geophysics)

Analysis of Long-term Borehole and Seafloor Pressure Data Recorded by the Subseafloor Observatories in Middle Valley, Northern Juan de Fuca Ridge. (May 2013)

Abstract of a dissertation at the University of Miami.

Dissertation supervised by Professor Keir Becker.
No. of pages in text. (92)

Pressure data recorded by long-term subseafloor observatories (CORKs) are a useful tool for understanding the state of the crustal hydrologic system. In Middle Valley, a sedimented rift at the northern end of the Juan de Fuca Ridge, thickly sedimented basaltic crust hosts an array of hydrologic regimes that have been monitored continuously by two CORKs since 1996. This dissertation analyzes both recent trends in borehole and seafloor pressures, as well as several older datasets, in concert with local seismicity, physical properties of the crust, and hydrothermal circulation in an effort to understand the region's ongoing dynamic eruptive cycle and hydrogeologic connectivity.

ACKNOWLEDGMENTS

"It is by knowledge that we prove, but by intuition that we discover."

- Henri Poincaré

Throughout my (almost lifelong) journey into geology, the deep sea, and hydrothermal systems, I have always wanted to be an explorer. Maybe it was all the *Star Trek* and *Dr. Who* I watched as a kid, or maybe it was my constant reading of Clive Cussler's Dirk Pitt novels: describing exciting 'discoveries' and derring-do around the world. I knew I loved the ocean at a very early age – picnics at Odiorne Point on the New Hampshire seacoast always included tidepooling with my parents, lifting back mounds of seaweed to look for critters hiding beneath. But at age 11, while reading one of Bob Ballard's books about deep sea exploration, I saw a photo of a black smoker chimney and was so enthralled by how little we knew about them that I decided to focus on becoming a marine geologist. Twenty years later as I finish this dissertation and begin a career as a Ph.D., I feel like I'm finally becoming the explorer that I was somehow born to be.

I could not have made it to where I am now without the unfailing and boundless support supplied by my parents throughout my life. They pushed me to do better, learn more, *be* more than I ever dreamed of as a kid growing up in rural New England. They gave me the ability to try going to sea on a tall ship with *SEA*, do fieldwork in Hawai'i as part of the JASON Project, and even try out a summer term at a university to see if I was ready. Through my bachelor's, my master's, and my doctorate they have continued to back me up, even during my decision to switch graduate schools which meant a delay to getting

my doctorate. They have always wanted what's best for me. I cannot ever thank them enough for being the best parents anyone could ever have.

I also am eternally indebted to my Ph.D. advisor, Keir Becker. When I returned to RSMAS I was a jaded, broken, washed-up geochemist. Keir has given me the freedom, guidance, and knowledge I needed to become a better scientist. He has also given me the opportunity to do extensive fieldwork at sea using ROVs and the DSV *Alvin*, as well as taking part in scientific drilling expeditions aboard the *JOIDES Resolution*. I told Keir early on that I wanted to be a seagoing chief scientist eventually, and he has given me every available chance to be involved in all aspects of our cruises, including sending me to accomplish all the geophysical goals at sea in 2010 when none of the PIs could sail. Keir also introduced me to the tightly-knit group of CORK scientists whom I now call my "science family." It has been a joy working with him for the last six years, and I am so glad that I will get to work with him in the future.

My committee has also been instrumental in aiding with the development of my research: Tim Dixon and Guoqing Lin with the modeling in Chapters 6 and 7, and Earl Davis with expanding my understanding of CORK pressure records and their implications for the hydrogeological system. Their critical analyses of my work have improved it greatly.

Outside of my committee, many colleagues have provided data, constructive discussions, and/or feedback on my work. Among these are Bob Meldrum, Martin Heeseman, Maurice Tivey, Norm Farr, Bob Dziak, Rob Sohn, and John Hildebrand. In addition a special thank you goes to my "science family" of colleagues: Andy Fisher, Geoff Wheat,

Katrina Edwards, Brian Glazer, Beth Orcutt, Alison LaBonte, Sam Hulme, and Dustin Winslow, for their support and encouragement throughout my Ph.D. and beyond.

I would be remiss if I did not thank the UM Geological Sciences faculty for providing me with the base knowledge to achieve this long-term goal of mine. John Southam, Fred Nagle, Larry Peterson, Jackie Dixon, and Hal Wanless taught me everything I know about geology, both in theory and in the field, and gave me the confidence to ask the tough questions.

Finally, I must thank my dear friends both at and outside of RSMAS: the RSMoids for our mutual griping/coping at the Wetlab and elsewhere, and my 'Canes baseball and costuming friends for keeping me sane when I wasn't working (yeah, Team Awesome!). And a very special thank you goes to my dear Mark: you've been my rock and my sounding board; you let me rant all over the place, and then remind me that I am an awesome scientist. You make me feel certain that I can do anything I set my mind to. I cannot thank you enough for your support, kindness, and friendship over the years.

TABLE OF CONTENTS

LIST OF FIGURES

LIST OF TABLES

CHAPTER ONE

INTRODUCTION

Fluid flow within the porous volcanic layer of oceanic crust may be one of the most influential, yet poorly understood processes on Earth. Fluid flow has the potential to influence the thermal and chemical evolution of the lithosphere, support subseafloor biological communities, and create ore-grade mineral deposits (eg. Alt, 1995; Davis et al., 1987), but we have yet to understand or quantify the parameters of this flow. The prevailing model of heat flux on young ocean crust (Stein and Stein, 1994) revealed that high temperature hydrothermal venting near mid-ocean ridge axes (crustal age < 1 Ma) is responsible for a mere fraction of heat lost by the cooling plate. In addition, the model accounts for the role of a sediment blanket that limits communication between the crust and the ocean. At many ridge axes basement is exposed extensively, allowing seawater to enter the porous crust easily. However as the crust ages, sediments accumulate and insulate volcanic basement from large seawater influxes and allow fluid circulation to continue, potentially for millions of years (eg. Elderfield et al., 1999). Recharge and discharge of fluids in thickly sedimented regions are controlled by basement bathymetry (Davis et al., 1989), with local highs as discharge zones and lows as recharge zones. However, despite the knowledge gained through modeling and heat flow studies, fluid circulation in ocean crust is not quantified.

It was the effort to understand fluid flow within ocean crust that drove scientists to develop long-term subseafloor observatories called Circulation Obviation Retrofit Kits (CORKs) (Davis et al., 1992). By deploying these instruments in boreholes drilled on the Juan de

Fuca Ridge by the Ocean Drilling Program (ODP), information about thermal, chemical, hydrological, and even biological processes in basement could be collected. The initial sites for the very first CORKs installed in 1991 are located in Middle Valley, a sedimented ridge segment at the northern end of the Juan de Fuca Ridge, selected not only for its thick blanket of sediment, but also the presence of a robust, high temperature hydrothermal system.

This dissertation will expound upon fluid pressure data obtained from the Middle Valley CORKs, as well as bring to light several unprecedented and significant observations derived from analyses of the long-term datasets available from Middle Valley.

CHAPTER TWO

STUDY AREA

2.1 Middle Valley

Middle Valley is a well-sedimented axial rift located at the northern end of the Juan de Fuca Ridge, just south of the Sovanco Transform and the Nootka Fault (Figure 2.1). It is blanketed by a thick layer of sediment that varies from 200 m to 2 km, composed of Pleistocene age turbidite deposits and hemipelagic sediment. The valley lies roughly along the axial strike of the unsedimented Endeavour segment located to the south. This, along with a relatively small amount of post-Pleistocene subsidence, indicates that Middle Valley was a primary center of spreading until recent times (Davis and Villinger, 1992). Local spreading is speculated to now occur in West Valley, a rift valley formed by ridge segment propagation, immediately west of Middle Valley (Davis and Villinger, 1992), although geologically young igneous intrusions in Middle Valley have also been observed (Davis and Becker, 1994).

1. Tectonic Structure and Sedimentation

Middle Valley is morphologically different than the magmatically robust Endeavour segment (~6 cm/yr full spreading rate); it exhibits the morphology of a much slower spreading ridge. This is likely due to decreased magma supply at the northern end of the segment (Davis and Villinger, 1992). Middle Valley is bounded on both sides by normal faults that have varying heights along the strike of the rift (Figure 2.2). Some of these faults have throws that expose a scarp above the valley floor, however many are completely buried or have little seafloor expression. In addition, depth to basement increases to the

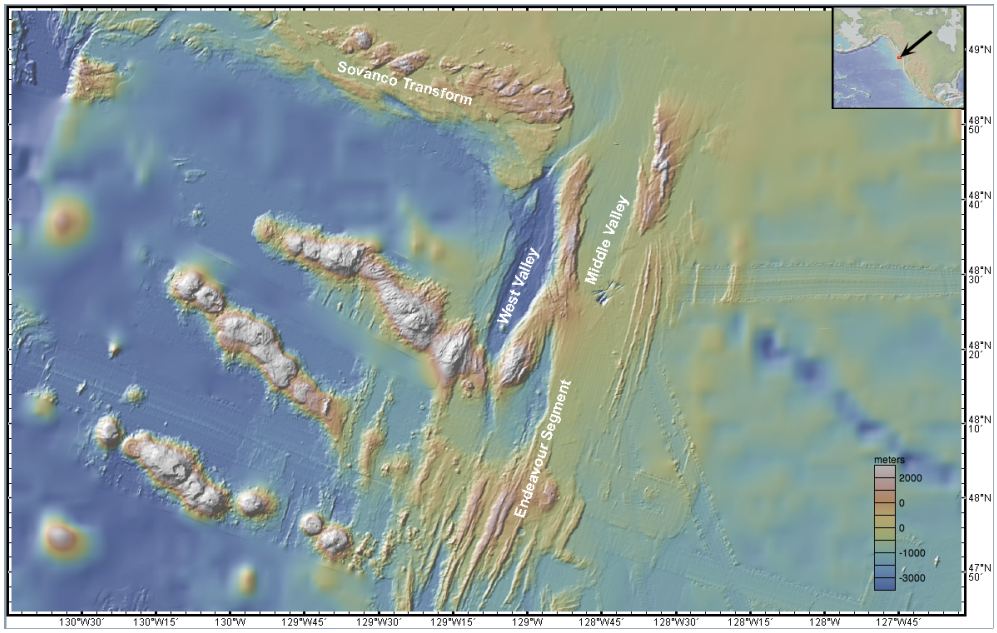

Figure 2.1 Map view of the northern Juan de Fuca Ridge. See text for location descriptions.

north, resulting in a thicker sediment section at the northern end of the rift valley (Davis and Villinger, 1992). The acoustically imaged sediment-basement interface is never sharp, implying a transitional boundary characterized by interbedded sediments and basaltic sills, which was observed at Site 857 (Davis and Becker, 1994).

Syntectonic sedimentation during the Pleistocene is responsible for the current bathymetry observed in Middle Valley. Turbidite deposits of silt and sand were observed in all holes drilled in Middle Valley, with graded beds and evidence of scouring (Shipboard Scientific Party, 1992a). Hemipelagic sediment was also observed, both interbedded with the turbidite sequences and as the dominant sediment type during the Holocene. Sediment bulk permeability was calculated to be 10^{-16} m^2 for representative samples (Fisher, et al., 1994).

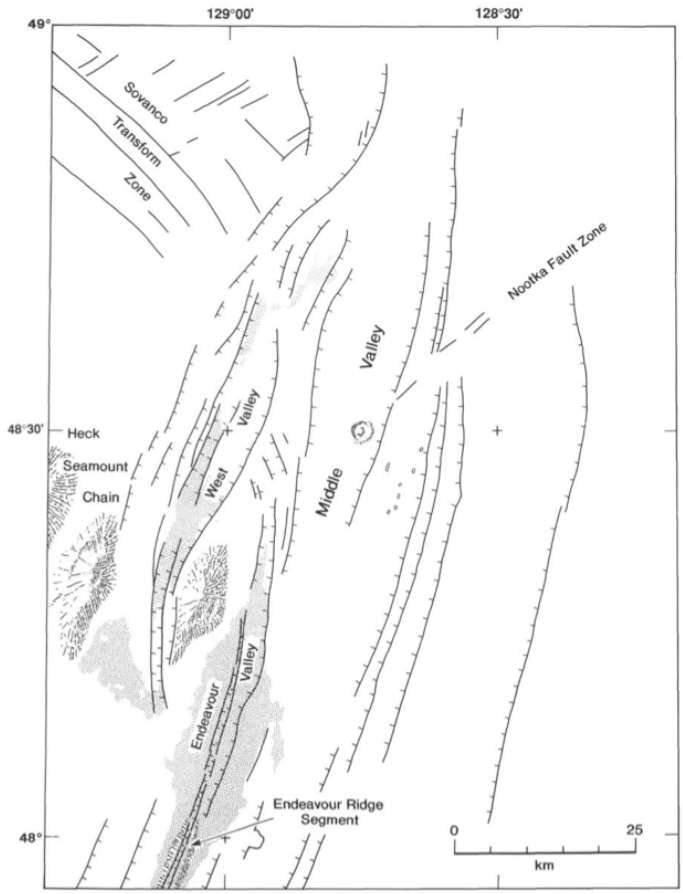

Figure 2.2 Tectonic interpretation of normal faults within Middle Valley. From Davis and Villinger, 1992.

2. Hydrothermal Features

Middle Valley hosts an array of hydrothermal features within the rift valley (Figure 2.3); including locations of both hydrothermal recharge and discharge. The Dead Dog vent field (Site 858) is an active field containing at least 20 vents that produce hydrothermal fluids up to 264°C (Ames et al., 1993). The Bent Hill Massive Sulfide deposit (Site 856, drilled during ODP Legs 139 and 169) ~4 km southeast of Dead Dog is a vent field that underwent high-grade alteration by high temperature fluids, producing a metal and sulfide rich ore-grade deposit (Shipboard Scientific Party, 1998b). Bent Hill encompasses a cylindrical volume ~60 m wide by ~120 m deep (Shipboard Scientific Party, 1998b). Underlying the

sulfide deposit are intensely mineralized and cemented sediments containing hydrothermal precipitates, followed by less altered turbidite sequences (Shipboard Scientific Party, 1998b). Fluids that discharge from a single vent 300 m south of the sulfide deposit are chemically similar to those that vent from the Dead Dog field (Butterfield et al., 1994) at a temperature of 265ºC.

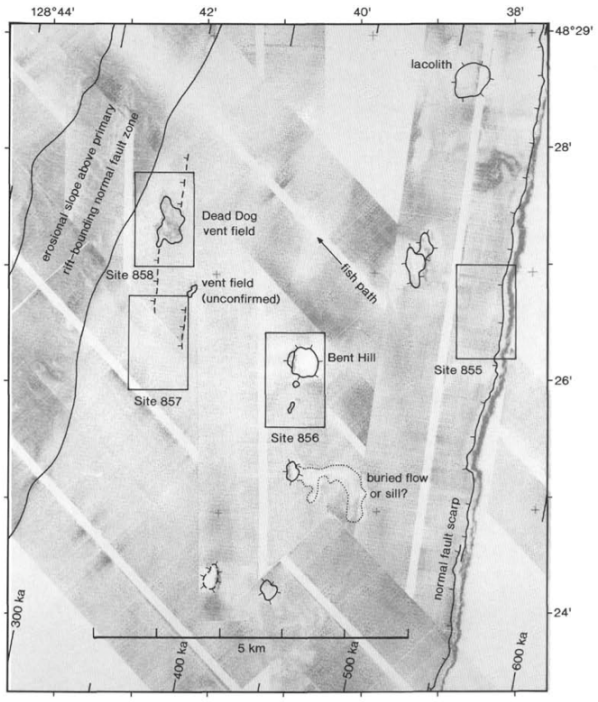

Figure 2.3. SeaMARC acoustic image mosaic of Middle Valley locations described in text. It is likely that the "unconfirmed vent field" consists of Puppy Dog and the 2 isolated chimneys. From Davis and Fisher, 1994.

Approximately 400 m southeast of the Dead Dog field (and 800 m northeast of Hole 857D) is a diffuse flow vent known as Puppy Dog. Puppy Dog hosts a significant biological community comprised mainly of tubeworms. Near Puppy Dog are two isolated chimneys, first observed in 2005, that vented fluid around 270°C. These chimneys were believed to be consistently active until sometime between August, 2008 and June, 2010, and have been

sampled for both temperature and fluid chemistry several times over the course of operations in Middle Valley (Wheat, pers. comm.).

A hydrothermal recharge zone (Site 855) lies on the eastern boundary fault of Middle Valley, where an outcropping fault exposes basaltic basement along a seafloor scarp (Shipboard Scientific Party, 1992a). Local average sediment thickness is ~90 m and the offset on the fault is roughly 115 m, exposing basalt along the footwall of the fault. The fault dips at 45º toward the center of the rift valley and was shown to be a location for seawater recharge into the crust, based on pore fluid chemical profiles collected from a transect of holes perpendicular to the fault trace (Wheat and Fisher, 2007).

2.2 ODP Site 857

This site is located at the southern end of Middle Valley and was chosen as a representative 'sealed' region of basement through which hydrothermal flow occurs (Shipboard Scientific Party, 1992a). It lies on a back-tilted fault block 1.5 km east of the sediment-buried normal fault that forms the structural center of Middle Valley and lies within the thermal anomaly that runs parallel to the rift axis (Davis and Villinger, 1992). Sediment thickness at Site 857 is approximately 400-500 m. Local heat flow is approximately 1 W/m^2 (Davis and Villinger, 1992).

1. Hole 857D

Hole 857D extends to 936 mbsf and is cased to 574 mbsf, through 470 m of sediment and into a series of interbedded basaltic sills and sediment (Shipboard Scientific Party, 1992a). This sill/sediment sequence is similar to those observed at other sedimented ridges (e.g.

Guaymas Basin; Curray and Moore, 1982) and for the purpose of this work is considered 'hydrologic basement' (Davis and Becker, 1994). Sill margins exhibit low-grade hydrothermal alteration, likely by a low-temperature, weakly metalliferous fluid (Shipboard Scientific Party, 1992a). Petrology of sill basalts indicates that there were multiple magma sources: one of an N-MORB composition, and one transitional, or T-MORB (Stakes and Franklin, 1994). The uppermost three sills drilled at Hole 857D resemble basalts drilled at Site 855 (N-MORB), but the sills in the hole are generally dominated by a second magma type (T-MORB) and others contain basalts with compositions between the two magma types. This suggests that at least one other mantle source fed the Site 857 sill complex during emplacement in addition to the depleted Site 855-type magma (Stakes and Franklin, 1994).

Initial basement temperature recorded by logging tools (at nearby Hole 857C, due to poor logging conditions at Hole 857D) at 476 mbsf was 222°C, which was extrapolated to give an upper limit of 260°C for hydrothermal basement temperature (Shipboard Scientific Party, 1992a). Downhole flow in Hole 857D was rapid and immediate following drilling, thus perturbing the thermal state of the hole until it was deepened later in the cruise. Rates of downhole flow were estimated to be 10,000 L/min (Langseth and Becker, 1994). Packer experiments (slug and injection tests) in the lowest 180 m of Hole 857D indicate a basement bulk permeability of 1×10^{-14} m^2, giving the sill-sediment sequence a permeability comparable to the upper few hundred meters of basaltic basement observed elsewhere (Becker, Morin, and Davis, 1994). An unusually high permeability of 10^{-10} m^2, several orders of magnitude higher than previously observed in young igneous basement, was calculated for a highly hydraulically transmissive zone at 610-615 mbsf. This

transmissive zone is likely associated with a normal fault (Langseth and Becker, 1994) and is assumed to be responsible for the rapid downhole flow (Becker, Morin, and Davis, 1994). Temperature gradients and flowmeter measurements indicate that much of the water enters the formation between 610-615 mbsf, with additional possible inflow zones at 690 and 825 mbsf, inferred by observed spikes in the temperature gradient at those depths in the hole (Langseth and Becker, 1994).

Following drilling operations at Hole 857D a CORK was installed (Figure 2.4) for long-term pressure and temperature observation. Further operations at Hole 857D are outlined in Table 2.1.

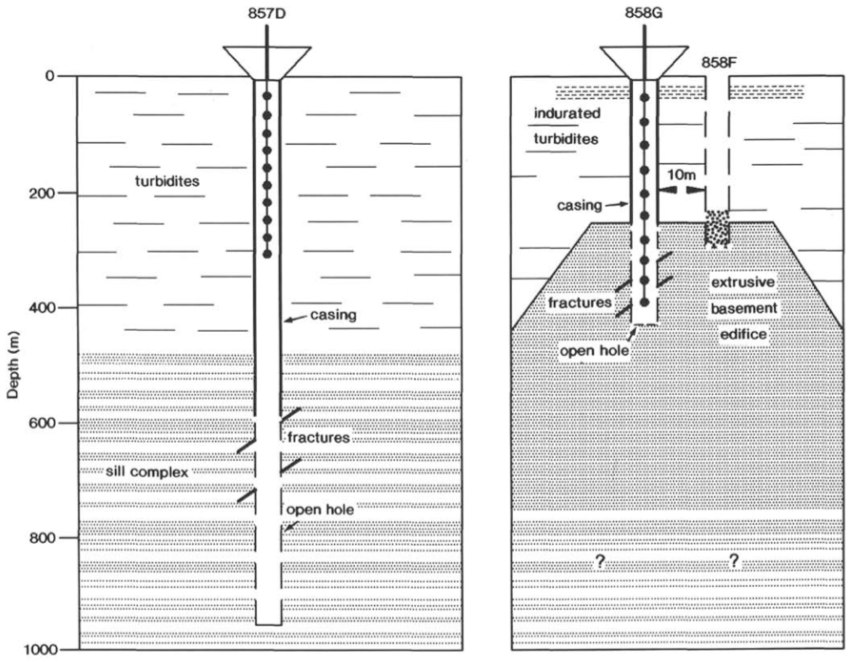

Figure 2.4. Cross sectional view of Holes 857D and 858G. The holes are 1.6km apart. From Davis and Becker, 1994.

History of Operations at 857D	
1991	ODP Leg 139: Hole is drilled to 954mbsf, single-seal CORK installed Alvin Dive 2457: Data Download
1992	ODP Leg 146: CORK is damaged during attempted thermistor string replacement
1996	ODP Leg 169: Damaged CORK is removed, downhole flow initiated and observed to 621mbsf Hole is re-CORKed without deepening (as previously planned)
1997	Alvin Dive 3146: Data Download
1999	Alvin Dive 3473: Data Download
2000	Alvin Dive 3608: Data Download
2003	JASON Dive: Data Download
2005	Alvin Dive 4155: Data Download
2007	Alvin Dive 4351: Data Download
2008	Alvin Dive 4431: Data Download
2010	JASON Dive J2-501: Data Download, new NEPTUNE compatible logger placed on platform
2011	JASON Dive J2-585: Data Download of NEPTUNE compatible logger only

Table 2.1. A detailed history of operations carried out on the CORK at Hole 857D

2.3 ODP Site 858

This site was chosen as a representative hydrothermal upflow zone within the southern portion of Middle Valley, as it is located over a local basement high and has a high local heat flow (Davis and Fisher, 1994). It is located 1.6 km north of Site 857 (Figure 2.3) within a hydrothermal field (Dead Dog field) that extends 800 m along and 400 m across the strike of Middle Valley. Site 858 is approximately 6 km east of the axis of the valley over an uplifted fault block buried by ~200 m of sediment (Shipboard Scientific Party, 1992b). Heat flow at the site reaches 20 W/m^2 in locations (Davis and Villinger, 1992).

1. Hole 858G

Hole 858G extends to 432 mbsf and is cased to 270 mbsf, through sediments and approximately 11 m of basement (Shipboard Scientific Party, 1992b). Unlike Hole 857D, Hole 858G does not have a transitional boundary between sediment and basement (Figure

2.4); basement is composed of apparently continuous basaltic flows and can thus be considered analogous to basement at unsedimented ridges (Becker, Morin, and Davis, 1994). Basalts from this hole are compositionally homogeneous, unlike the sills in Hole 857D, and contain spinels with compositions similar to those found in basalts in West Valley as well as overlapping spinel compositions from Hole 857D sills (Stakes and Franklin, 1994). This compositional overlap suggests that Hole 858G basalts formed from a slightly enriched mantle source that formed during the late stages of magmatism in Middle Valley and that also fed the sill complex at Site 857 (Stakes and Franklin, 1994).

Basement at Hole 858G is highly altered and fractured, and initial basement temperature recorded by logging tools at 162 mbsf was 268°C (Shipboard Scientific Party, 1992b). Packer experiments (slug and injection tests) at Hole 858G indicate a basement bulk permeability of 1-4 x 10^{-14} m^2, similar to the bulk permeability observed at the bottom of Hole 857D (Becker, Morin, and Davis, 1994). Induced downhole fluid flow (due to the difference between borehole and surrounding formation hydrostatic pressures) was calculated to be 150 L/min, two orders of magnitude less than downhole flow observed in Hole 857D (Langseth and Becker, 1994). Several highly transmissive zones were identified during flowmeter tests in the section between 320 and 350 mbsf, which have a calculated average permeability of 2-3 x 10^{-13} m^2 (Becker, Morin, and Davis, 1994).

Following drilling operations at Hole 858G, a single-seal CORK was installed (Figure 2.4) for long-term pressure and temperature observation. Further operations at 858G are outlined in Table 2.2.

History of Operations at 858G

1991	ODP Leg 139: Hole is drilled to 436 mbsf, single-seal CORK installed Alvin Dive 2457: Data Download
1992	ROPOS Dive: Data Download
1993	Alvin Dive 2665: CORK hydraulic seals failed, fluid venting is observed
1996	ODP Leg 169: CORK removed, hole isothermal (272°C) below 85 mbsf Anhydrite/pyrite/pyrrhotite recovered from inside casing Hole cooled and re-CORKed
1997	Alvin Dive 3146: Data Download
1999	Alvin Dive 3473: Data Download
2000	Alvin Dive 3608: Attempted data download, CORK not responding

Table 2.2. A detailed history of operations carried out on the CORK at Hole 858G

CHAPTER THREE

THE CORK PROGRAM

3.1 Motivation

The initial goal of the CORK program was simple: to develop the technology to monitor in-situ fluid pressure and temperature within sediments and crust over extended periods of time. The obvious way to accomplish this was to make measurements in ODP holes, some of which historically had penetrated permeable crust. However as a consequence of circulation during drilling, formation pressure is perturbed by the cold, dense seawater injected into the warm, less dense formation fluid (Davis et al., 1992). This prevents logging and many downhole measurements from being completely accurate, as observed at Hole 857D during Leg 139 (Becker, Morin, and Davis, 1992). In cases of formation underpressure, as often observed to be the case in holes drilled into young oceanic crust, drilling-induced downhole flow effectively 'short circuits' the system after drilling operations have ceased. Leaving an underpressured hole open to seawater flow following drilling operations can severely contaminate the local formation. In cases of formation overpressure, the hole has a better chance of recovering from drilling perturbations over time, however what is essentially a synthetic vent may be created and may affect local hydrothermal circulation (Davis and Becker, 1999). Thus, CORKs were designed to hydrologically seal fluids in the formation from the seawater column above. This allows the formation to recover from the thermal and chemical effects of drilling and return to pre-drilling conditions, while in-situ hydrological conditions can be monitored long-term (Davis et al., 1992).

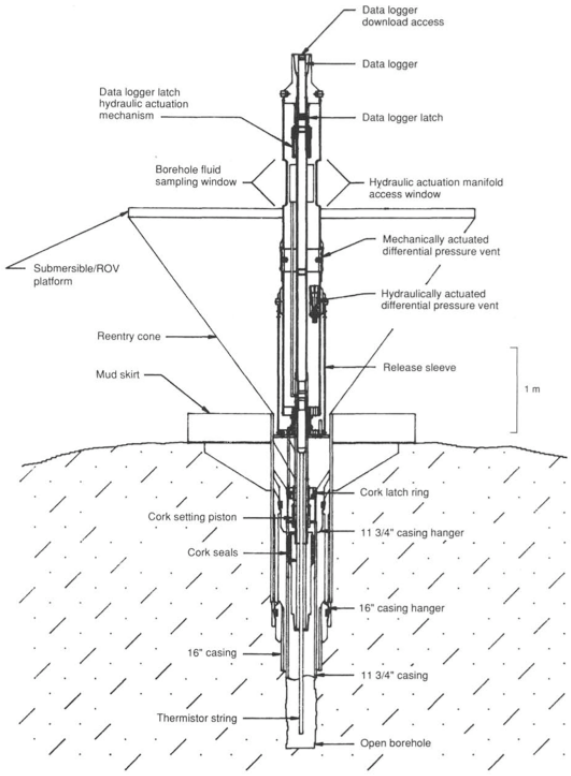

Figure 3.1. Schematic diagram of an original single-seal CORK. From Davis et al., 1992.

The design for the original CORK is shown in Figure 3.1. Single seal original CORKs contained only pressure gauges, a thermistor string, and a borehole fluid sampling tube as downhole instrumentation. The original design has changed since 1991 and continues to evolve as technology advances and we develop more complex experiments to run on the crustal hydrologic system (e.g. Fisher et al., 2005).

3.2 Pressure Records

Each CORK pressure data logger is programmable: the sampling rate can be changed if necessary. Following the initial deployment in 1991, Hole 858G was set to record pressure every ten minutes. This was changed to once per hour during the first data download in 1991 (Davis and Becker, 1994). Sampling rate at Hole 857D was also adjusted from once

per hour to once every ten minutes for ~2 years of monitoring (2003-2005). The newest generation of data loggers is capable of up to 1 Hz sampling and is compatible with existing cabled seafloor observatory platforms (i.e. NEPTUNE Canada).

A remarkable initial observation about borehole pressure was that it responds to tidal loading forces just as seafloor pressure does. Within the formation the ocean tidal load is partitioned between the rock matrix and interstitial fluids based on their elastic properties (ratio of bulk moduli, matrix porosity). The amplitude of the borehole signal is attenuated and the amount of attenuation is the loading efficiency of the formation (Wang and Davis, 1996): defined numerically as the fraction of total pressure change accommodated instantaneously (elastically) by the interstitial fluid. For example, a highly compressible formation matrix (such as highly fractured rock) will exhibit little tidal signal attenuation (i.e. a large loading efficiency) because the fluid must accommodate a larger share of the load. In contrast, a less compressible formation matrix will have a highly attenuated pressure signal (i.e. a smaller loading efficiency) due to the matrix accommodating a greater share of the load. A formation's loading efficiency is one-dimensional and zero phase, meaning no net fluid flow (Wang and Davis, 1996). If we also consider a formation's three-dimensional hydraulic diffusivity in addition to its elastic properties, we see that an internal contrast in matrix compressibility (and thus loading efficiency) over short path length creates an instantaneous pressure difference, leading to Darcy flow across the interface and diffusion waves propagating in both directions across it (Wang and Davis, 1996). Depending on the distance from this interface, a phase lead or lag in the pressure signal may result from the diffusive perturbation to the elastic component of loading (Wang and Davis, 1996). Owing to the apparent anisotropy of the porous oceanic crust, elastic

property and porosity contrasts due to fracture density and/or lithology are likely prevalent on varying length scales. Thus, tidally driven fluid motion is probably a common process on multiple scales within the crust (Wang and Davis, 1996).

3.3 Seismic Events

In addition to tidal loading experienced by the formation, local and distal seismicity can perturb the background pressure state of the hydrologic system. This has been observed in the pressure records of many CORKs. In the case of Middle Valley, the effects of local earthquake swarms were recorded in 1991, 2001 (Davis et al., 2004), and 2004 and a distal swarm was recorded in 1999 (Davis et al., 2001). The effect of an earthquake swarm on a borehole pressure record is a function of the CORK's location relative to the strain field created by the earthquake. The presence of a pressure increase or decrease reflects whether the CORK's location was subjected to the compressional or dilatational quadrant of the strain field; where compression produces a pressure spike and dilatation produces a pressure drop in the record. For example, the 2001 Endeavour swarm caused a rapid 12kPa drop in borehole pressure at Hole 857D (Figure 3.2A) (Davis et al., 2004), however the 1999 Endeavour swarm produced pressure spikes at CORKs on the eastern flank of Juan de Fuca and a small pressure drop at Hole 857D (Figure 3.2B) (Davis et al., 2001).

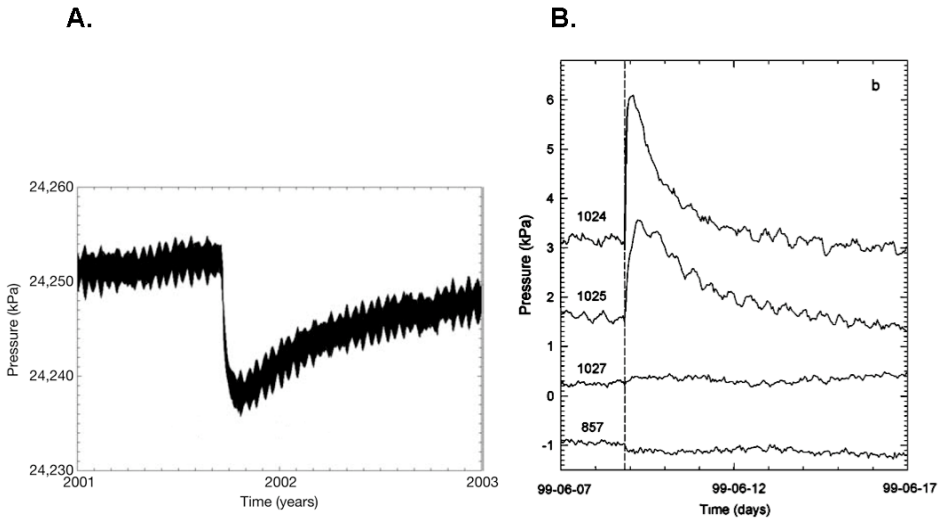

Figure 3.2 A: Pressure response in Hole 857D following a 2001 earthquake swarm on the Endeavour segment. From Davis et al., 2004. **B.** Pressure response in multiple Juan de Fuca CORKs following a 1999 earthquake swarm on the Endeavour segment. From Davis et al., 2001. Note that while tidal frequencies have not been removed from 6A, 6B's pressures are corrected for tidal forces.

The subtlety of many pressure responses to earthquakes makes it difficult to look for them directly. Real-time seismic data is collected by the Sound Surveillance System (SOSUS) hydrophone buoys in the northeast Pacific and can be used to pinpoint swarms that may affect the CORK network on Juan de Fuca (Fox et al., 1994). This allows for the more subtle seismic responses to be teased out of a CORK's borehole pressure record. The SOSUS array does have limitations: the buoys cannot detect earthquakes with magnitudes under 2.4, however having a network of buoys that collect real-time seismic data has been invaluable in the interpretation of borehole pressure records. Additional Ocean Bottom Seismometer (OBS) arrays have been deployed in the region throughout the history of the CORK program (eg. 1996 Middle Valley array, 2003-2007 Keck Seismic Network) and provide additional sources for data on local and distal seismicity.

CHAPTER FOUR

REMOVAL OF OCEANOGRAPHIC EFFECTS WITH MATLAB

4.1 Motivation

In order to identify and analyze small pressure transients within pressure records obtained from CORK observatories, it is critical that oceanographic effects be removed from the record, most importantly the effects due to tides. The reason for this is simple: loading due to tides is observed both in the seafloor and formation pressure data, and this load imposes a large overprint on any minor pressure changes, making only the most obvious pressure changes visible in an uncorrected record. In the case of the Juan de Fuca region, the area is subject to a significant tide that is commonly 2 m in amplitude between high and low stands (Davis and Becker, 1994). Two meters of net change in water height represents 20 kPa of pressure change, thus overprinting any small pressure transients due to seismic or other disturbances. It is important to note that tidal loading on formation pressure occurs in-phase with the local tidal cycle and that this load is partitioned between the rock matrix and the fluids present in the porous crust. The ratio of this partitioning (fluid:matrix) is defined as the loading efficiency of the formation (Wang & Davis, 1996). Additionally, any diffusion occurring within the formation may cause a phase lead or lag of the interstitial fluid pressure response, as described previously. This chapter will outline the process by which tidal signals were removed from both formation and seafloor pressure records obtained from CORKs for this study.

4.2 T_tide MATLAB Code

T_tide is a freely available MATLAB code used for predicting tides based on a given periodic dataset (Pawlowicz, Beardsley, & Lentz, 2002). Given inputted data and a known sampling rate, the code will generate a "best fit" tidal signal for the given values by calculating a set of tidal constants. An example of the tidal constants output from the code is in Table 4.1. T_tide was not designed for analysis of long-term datasets (unless greater than 19 years), thus the records analyzed in this dissertation were broken into sections of length of one year or less for analysis. Additionally, an issue unmentioned by Pawlowicz et al. (2002) is the relative inability of T_tide to comprehend long-term, linear data trends in a record; the sinusoid generated from these year-long records in no way resembles a tidal cycle. An example is shown in Figure 4.1. In the case of such a linear trend existing in these data, the record was cut into sub-annum parts (to be analyzed separately) in order to generate a proper tidal sinusoid. At this time, shortening the record length appears to be the only workaround for this limitation in the existing MATLAB code.

4.3 Method: Formation Pressure Record

Step 1: Calculation of Loading Efficiency:

Given a pressure dataset from a CORK (example: Figure 4.2A), the first matter is to determine the loading efficiency for the formation at each CORK site. This is accomplished by generating a cross-plot of formation pressure and seafloor pressure deviations from the average over a complete tidal cycle (in this case, 2 months worth of data were used: Figure 4.2B). Generating a linear regression through this cross-plot yields the loading efficiency, which is the slope of the regression line (Wang and Davis, 1996)

```
nobs = 12960,  ngood = 12959,  record length (days) = 90.00
rayleigh criterion = 1.0
Phases at central time

x0= 2.07e+004, x trend= 0

var(x)= 0.21397   var(xp)= 0.0064949   var(xres)= 0.20747
percent var predicted/var original= 3.0 %

     tidal amplitude and phase with 95% CI estimates
```

tide	freq	amp	amp_err	pha	pha_err	snr
MM	0.0015122	0.1620	0.181	139.12	69.60	0.8
MSF	0.0028219	0.1300	0.175	279.34	94.37	0.55
ALP1	0.0343966	0.0061	0.006	309.46	66.36	1.1
2Q1	0.0357064	0.0063	0.006	77.97	58.12	0.99
*Q1	0.0372185	0.0141	0.007	259.17	30.00	4.1
*O1	0.0387307	0.0658	0.006	143.77	6.92	1.1e+002
*NO1	0.0402686	0.0095	0.007	38.32	41.21	2
*K1	0.0417807	0.0686	0.007	264.53	6.55	1e+002
*J1	0.0432929	0.0097	0.006	164.75	39.06	2.5
OO1	0.0448308	0.0068	0.006	114.75	63.11	1.2
UPS1	0.0463430	0.0045	0.006	288.58	87.54	0.62
EPS2	0.0761773	0.0038	0.003	37.68	50.83	1.6
MU2	0.0776895	0.0038	0.003	313.47	46.11	1.5
*N2	0.0789992	0.0150	0.003	343.54	11.15	26
*M2	0.0805114	0.0561	0.003	249.62	3.74	3.9e+002
L2	0.0820236	0.0033	0.003	94.98	55.74	1.2
*S2	0.0833333	0.0183	0.003	105.54	10.49	32
ETA2	0.0850736	0.0025	0.003	257.29	76.69	0.71
*MO3	0.1192421	0.0030	0.002	196.01	36.47	2.5
*M3	0.1207671	0.0039	0.002	81.83	32.62	3.4
*MK3	0.1222921	0.0039	0.002	322.13	31.59	4
SK3	0.1251141	0.0028	0.002	286.87	36.35	1.9
MN4	0.1595106	0.0021	0.002	353.71	58.69	1.5
M4	0.1610228	0.0027	0.002	233.45	43.24	1.7
SN4	0.1623326	0.0019	0.002	32.84	58.78	1.3
MS4	0.1638447	0.0015	0.002	247.63	79.62	0.75
S4	0.1666667	0.0026	0.002	268.75	41.86	1.6
2MK5	0.2028035	0.0022	0.002	257.54	61.09	1.4
2SK5	0.2084474	0.0004	0.001	194.38	172.72	0.1
2MN6	0.2400221	0.0005	0.002	276.10	189.61	0.082
M6	0.2415342	0.0006	0.002	196.09	168.91	0.13
2MS6	0.2443561	0.0012	0.002	225.56	100.90	0.45
2SM6	0.2471781	0.0017	0.002	236.67	71.94	0.96
3MK7	0.2833149	0.0010	0.001	241.83	96.15	0.57
M8	0.3220456	0.0001	0.001	146.22	228.93	0.013

Table 4.1. T_tide output for 90 days of data from 2005. Constants (at left) are calculated with 95% confidence.

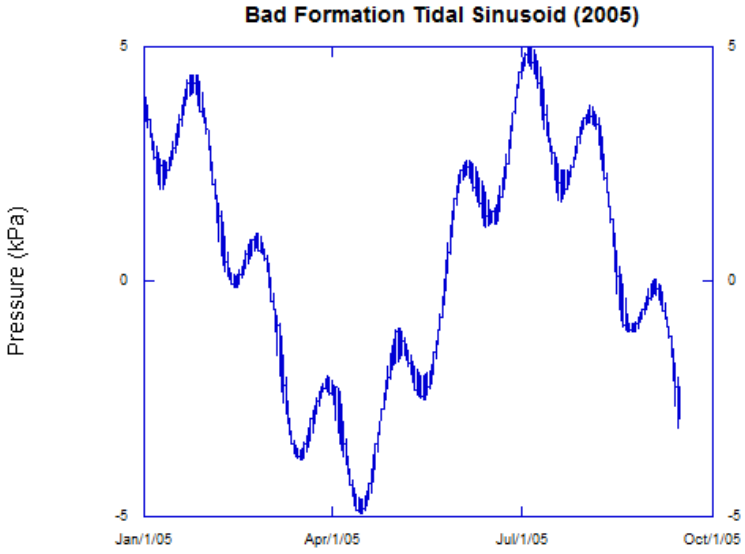

Figure 4.1. Bad tidal sinusoid generated for a portion of the formation record with a linear trend (2005).

that appears to differ slightly for diurnal and semi-diurnal phases (note the change in slope in Figure 4.2B data), indicating there is some phase or Earth tide that cannot be ignored. In other words, the value calculated here is the percent of seafloor load that is "felt" by the formation matrix. In the case of Hole 857D, the formation pressure signal is highly attenuated and only experiences 14% of direct seafloor loading.

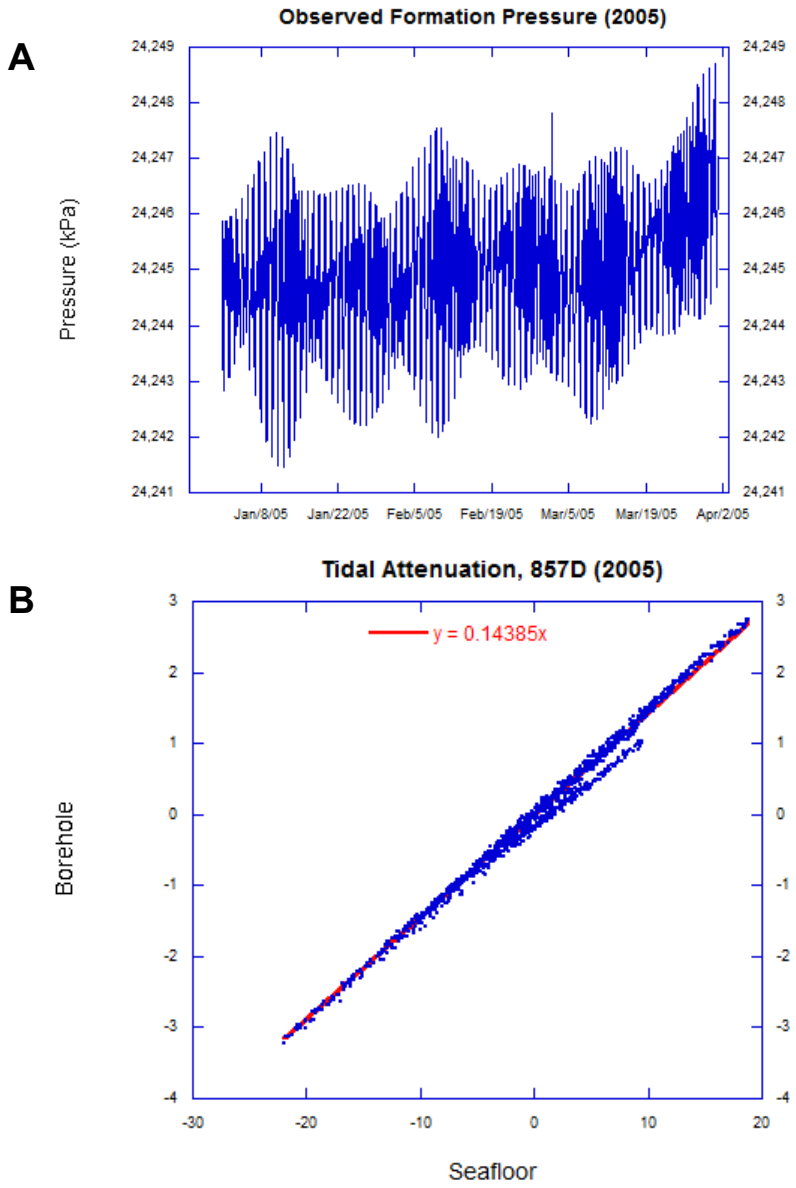

Figure 4.2 A. Original formation pressure record from Hole 857D (2005). **B.** Cross-plot of formation and seafloor tidal magnitudes (difference from zero) from Hole 857D in 2005. Note the apparent slope change. Linear regression of these data produces the formation's loading efficiency.

Step 2: Removal of Seafloor Loading:

Using the loading efficiency previously calculated, the percentage of the seafloor pressure directly felt by the formation matrix is subtracted from the total formation pressure. Effectively:

Unloaded Formation P = Formation P - [(Loading Efficiency %)(Seafloor P)]

The generated corrected formation pressures will still show some periodicity, which is either due to diffusion in the formation or an Earth tide component. If the response to loading was purely elastic, there would be no residual component. The source of this residual periodicity is not yet clear, but the residual will be removed in the next step.

Step 3: Removal of Residual Periodicity:

Using the unloaded formation pressure record generated in step two and the sampling rate, run T_tide to predict tidal constants and produce a sinusoid (Figure 4.3A) representing tidal loading experienced by fluids contained within the formation matrix. The generated sinusoid should be inspected to ensure the viability of the predicted data, especially in cases of data with linear trends, as mentioned previously. Finally, subtract the predicted data from the unloaded formation pressure data to get a corrected formation fluid pressure record (Figure 4.3B).

Corrected Formation Fluid P = Unloaded Formation P – Predicted P

Some small amount of periodicity may still be present depending on the prediction accuracy of the tidal constants, however this process removes most of the excess pressure changes that overprint any subtle changes in the formation record.

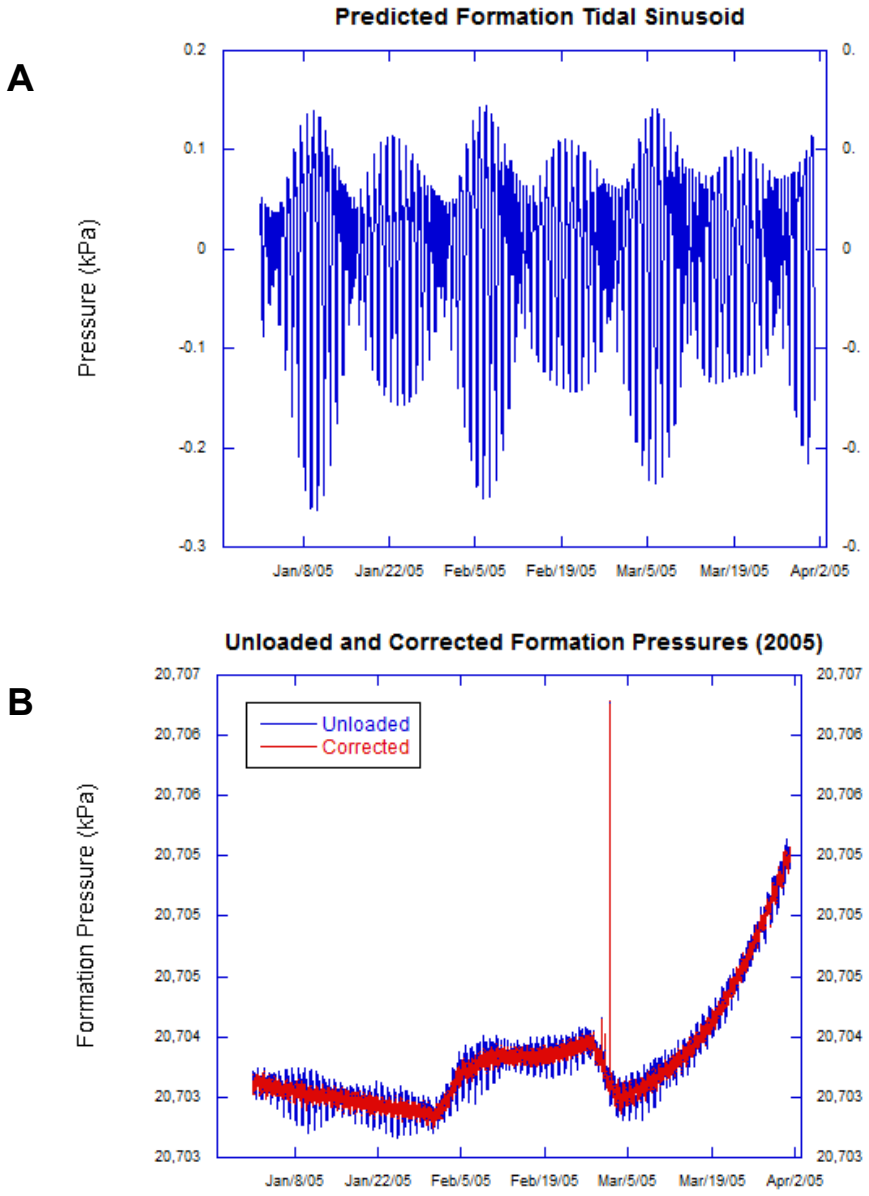

Figure 4.3 A. T_tide predicted tidal sinusoid for Hole 857D (2005). **B.** Plot comparing the unloaded formation record determined in step 2 to the corrected record that reflects removal of tidal forcing determined in step 3.

4.4 Method: Seafloor Pressure Record

Removing tidal influences from the seafloor record is a much simpler process than that of the formation record. T_tide is run directly on the seafloor pressure data, generating a tidal

sinusoid (which is checked for viability) and the resultant predicted pressure is subtracted from the original seafloor pressure (Figure 4.4).

$$Corrected\ Seafloor\ P = Seafloor\ P - Predicted\ Seafloor\ P$$

Once again, the corrected data will likely show some residual noise or periodicity as a result of the accuracy of the tidal constants predicted by T_tide.

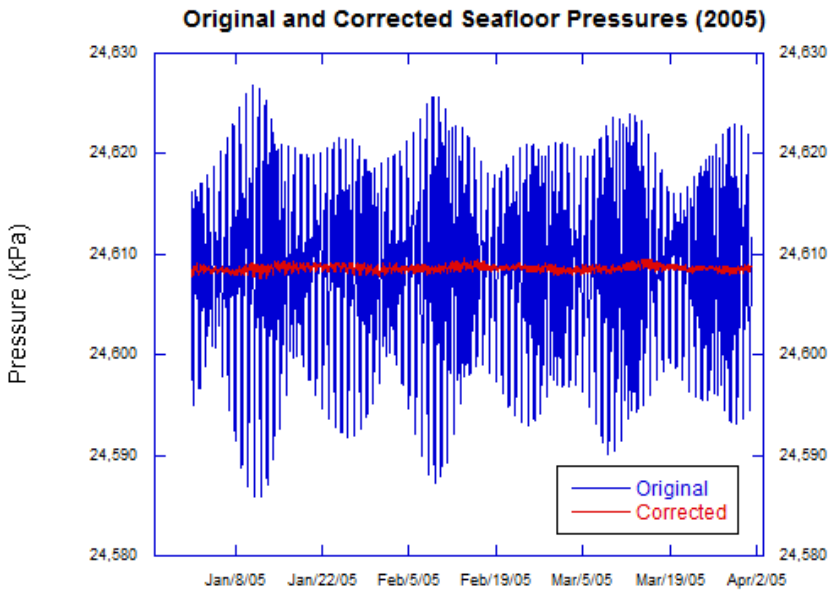

Figure 4.4. Comparison of original and corrected seafloor pressure (2005).

CHAPTER FIVE:

A SUBSEAFLOOR OBSERVATORY RECORD OF SEAFLOOR "UPLIFT" IN MIDDLE VALLEY, 2005-2010

5.1 Motivation

Over the past two decades, extensive research has been conducted regarding the effects of geological phenomena on mid-ocean ridge and ridge flank subseafloor hydrogeology utilizing long-term, subseafloor observatories (CORKs) installed by the Ocean Drilling Program (ODP) and the Integrated Ocean Drilling Program (IODP) (eg. Davis and Becker, 1994; Davis et al., 2004; Fisher et al., 2011). The two earliest CORKs were installed in Middle Valley, a sedimented spreading center on the northern Juan de Fuca Ridge, to monitor fluid pressure within the crust and at the seafloor in an attempt to understand and quantify the hydrologic connectivity and convective vigor within basaltic basement. The axial rift there is host to high-temperature hydrothermal venting, seawater recharge along bounding faults, and sediment-hosted, massive sulfide mounds. The 15 year record of pressures from Hole 857D is currently one of the longest continuous records of subseafloor formation pressure available for analysis. In this chapter we present exciting evidence of potential seafloor uplift from the most recent 6 years of pressure monitoring in Middle Valley.

5.2 Geologic Setting

Middle Valley has been the subject of two ODP expeditions (139 and 169) and contains a suite of hydrologic regimes: active hydrothermal venting from overpressured basement

with underpressures at shallow levels at Dead Dog field (ODP Site 858/1036), a massive sulfide mound at Bent Hill (ODP Site 856/1035) that is also actively venting from overpressured basement, seawater recharge at boundary faults (ODP Site 855) and Site 857, which is located at the southern end of Middle Valley (Figure 5.1) and was chosen as a representative sediment-sealed region of basement through which hydrothermal flow occurs (Shipboard Scientific Party, 1992a). Sediment thickness at Site 857 is approximately 400-500m and basement exhibits a ~300 kPa underpressure relative to the seafloor hydrostatic.

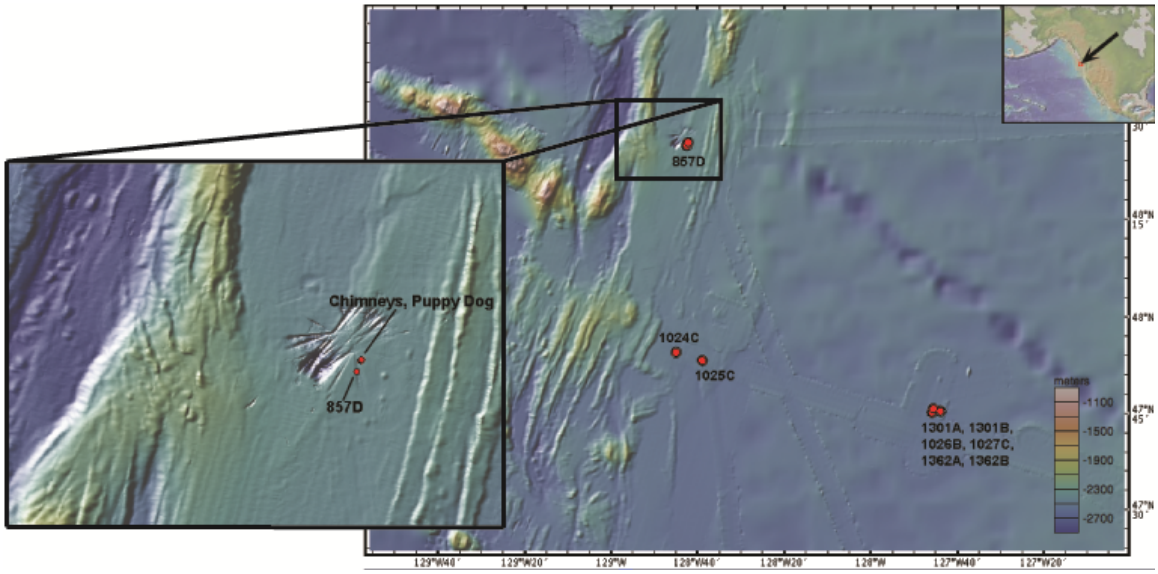

Figure 5.1. Map of CORKs installed on the Juan de Fuca Ridge. Inset is Middle Valley and shows its associated features. Generated with GeoMapApp. Note that some linear bathymetric features that appear are artifacts, such as the linear divots in southern Middle Valley.

Hole 857D, initially drilled in 1991, extends to 936 mbsf and is cased to 574 mbsf through 470m of sediment and into a series of interbedded basaltic sills and sediment (Shipboard Scientific Party, 1992a). This sill/sediment sequence is similar to those observed at other sedimented ridges (eg. Guaymas Basin; Curray and Moore et al., 1982) and is considered 'hydrologic basement' (Davis and Becker, 1994). Hole 857D was

drilled to recover basalt samples, to allow hydrologic testing via a drillstring inflatable packer, and for the purpose of installing a long-term subseafloor observatory (CORK). A single-seal CORK was installed for long-term pressure and temperature observation (Davis and Becker, 1994). The upper CORK body was later damaged during a recovery attempt in heavy seas in 1992 (ODP Leg 146) and was ultimately replaced, along with the downhole string, during ODP Leg 169 in 1996 (Fouquet, Zierenberg et al., 1998).

5.3 Data: Pressure Record Description and Significant Events

The CORK at Hole 857D has been visited periodically since 1996 by DSV Alvin and the ROV JASON for the purpose of downloading pressure data from the internal logger. In addition, a new pressure monitoring system with a data logger was installed on the CORK's formation fluid sampling port in June, 2010. The new logger is currently recording one concurrent borehole and seafloor pressure sample per minute, and is capable of 1Hz data sampling when supplied with outside power (eg. NEPTUNE Canada cable). Currently there is a 14 year continuous record (1991-1992, 1996-2010) of both seafloor and borehole pressures at Hole 857D, taken at an hourly sampling rate by the internal logger. The 14 year pressure record from Hole 857D's internal logger is shown in Figure 5.2. In order to examine any transients in the Hole 857D borehole pressure record, the effect of tides, which cause significant fluctuations in the pressure signal, must be removed. Please refer to Chapter 4, "Removal of Oceanographic Effects with MATLAB," for a detailed description of this process.

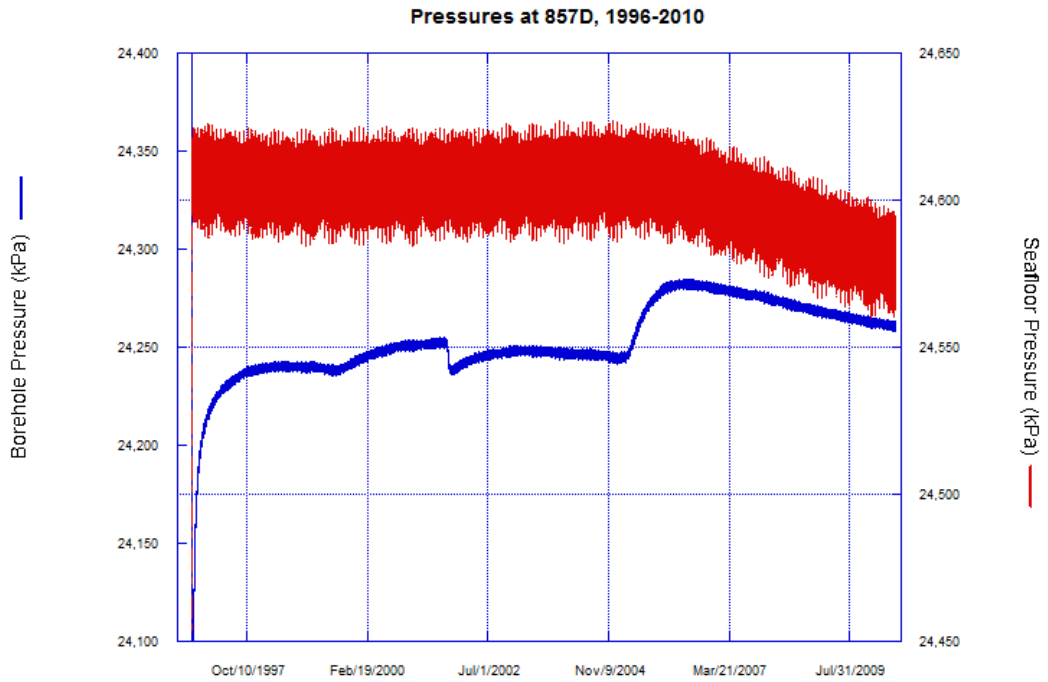

Figure 5.2. Fourteen-year record of pressures recorded by in the internal logger at 857D. Tidal effects have not been removed.

Several borehole pressure transients in the Hole 857D record have been attributed to the influence of seismic activity (e.g. Davis et al., 2001; Davis et al., 2004; Hooft et al., 2010) both locally in Middle Valley and more distally on the Endeavour Segment. Observations based on the most recent six years of data are the central focus of this chapter.

1. Internal Logger Data

The 2005-2010 pressure record from the internal Hole 857D logger is shown in Figure 5.3 with the effects of tides removed as previously described. Beginning in early March, 2005, borehole pressure began to rise rapidly at a rate of ~3.7 kPa per month. Borehole pressure jumped (0.8 kPa within an hour) on November 19 of the same year, and peaked shortly afterwards. Total pressure increase in the formation was ~40 kPa over the course

of 2005. This was followed by a gradual decrease in borehole pressure of ~20kPa that extended over the course of the following four years.

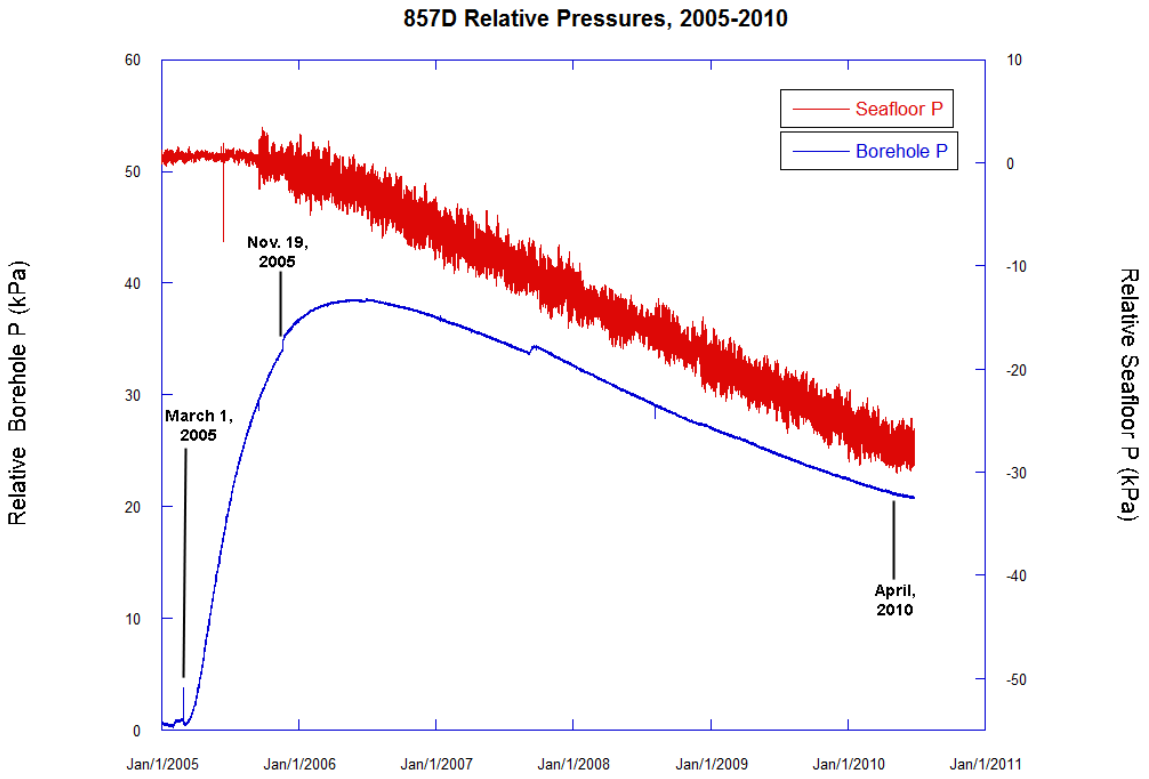

Figure 5.3. 2005-2010 relative pressure record from the internal logger at Hole 857D. Tidal effects have been removed. Events are further explained in the text.

Seafloor pressure at Hole 857D, which was relatively stable from the beginning of the record in 1996 through November, 2005, tracks the decrease in pressure experienced by the formation. Total decrease in seafloor pressure was ~27kPa (or ~2.7m of head) over the same time interval of borehole pressure decrease (November 2005 – July 2010). Note that the increase in "high frequency" noise during this seafloor pressure decrease is a result of data processing with T_tide, as long linear data trends are not handled well by the code (as noted in Chapter 3).

2. High-Resolution Logger Data

The new high-resolution data logger was downloaded for the first time in September, 2011. These data, shown with the effects of tides removed in Figure 5.4, show a relatively constant seafloor pressure and a slowly decreasing formation pressure, for the duration of the first year of deployment, following a post-installation recovery period. The formation record from this logger follows the same trend as the internal logger, which unfortunately was not downloaded in 2011; the constant seafloor pressure signal was unexpected and initially perplexing.

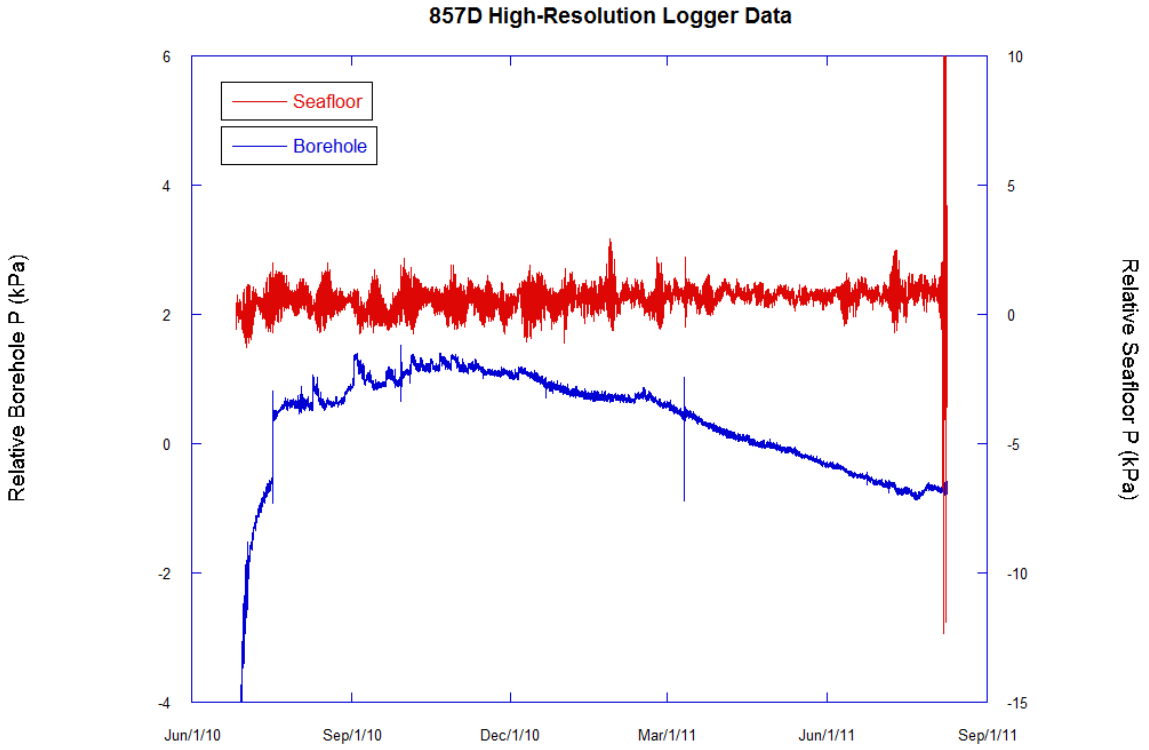

Figure 5.4. 2010-2011 relative pressure record from the high resolution logger at Hole 857D. Tidal effects have been removed.

Closer analysis of the end of the internal logger's seafloor signal in 2010, however, reveals a plateau in pressure that began roughly around April, 2010 (Figure 5.5).

Additionally, the rate of pressure decrease in the seafloor record is significantly lower in 2010 than for 2006-2009 (Table 5.1).

Year	Change in Seafloor Pressure (kPa)	Rate of Pressure Change (kPa/month)
2006	-5.205	-0.434
2007	-6.433	-0.536
2008	-6.878	-0.573
2009	-6.169	-0.514
2010*	-2.074	-0.346

Table 5.1. Rates of change of seafloor pressure between 2006 and 2010. Note the significant drop in rate of pressure change in 2010 as compared to the three previous years. *This rate is based on 6 months of data (Jan. - June) only, as opposed to 12 months for 2006-2009.

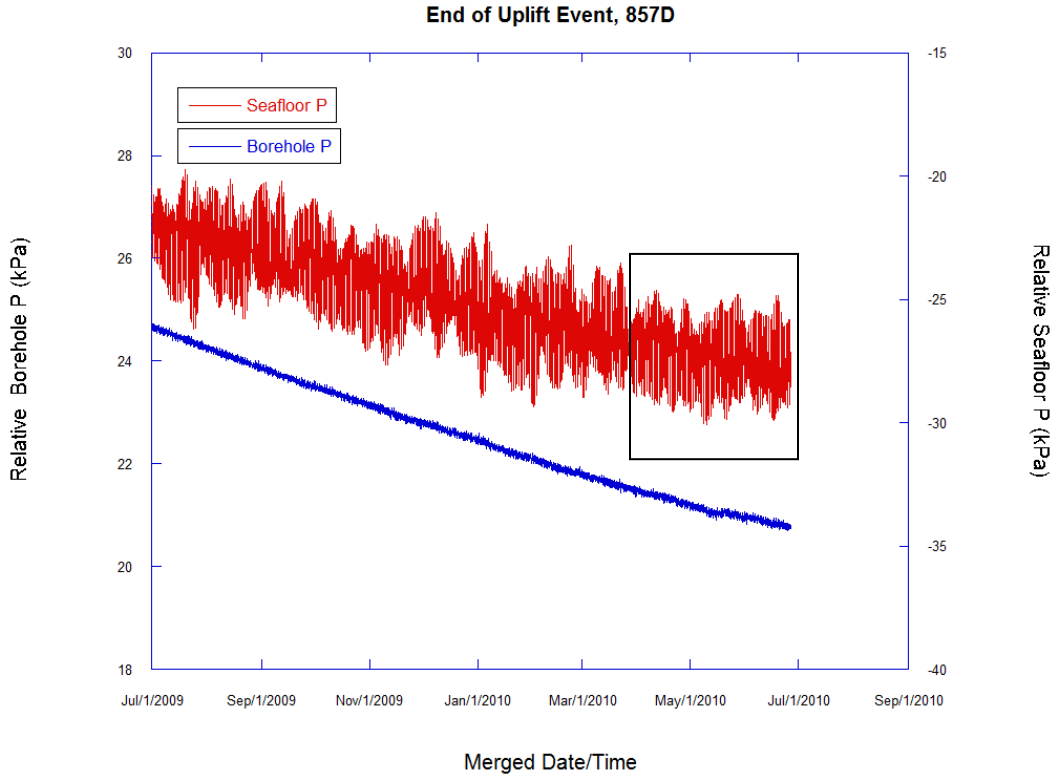

Figure 5.5. 2009-2010 relative pressure record from the internal logger at Hole 857D showing a plateau in seafloor pressure (inside box) starting in April, 2010. Tidal effects have been removed.

5.4 Interpretation

1. Physical Seafloor Uplift?

There are two potential causes for a decrease in the seafloor pressure record: 1) a change in drift of the Paroscientific gauge measuring seafloor pressure that is installed in the CORK body, or 2) reduction of water column height above the CORK. Following extensive analyses on the drifts of datasets from CORKs and other observing systems using Paroscientific pressure gauges by Polster, Fabian, and Villinger (2010), the CORK data were found to fit a linear drift model and inferred to have a constant drift for the duration of a deployment. The drift for the Paroscientific seafloor pressure gauge installed at Hole 857D was calculated as +0.74 kPa/annum (Polster, Fabian, and Villinger, 2010), which does not explain the seafloor pressure decrease (nearly 6 kPa/annum) recorded by the pressure gauge. The post-2006 linearity of both seafloor and formation records argues against any erroneous behavior confined to one gauge, as it would be exceedingly unlikely that both gauges would be affected at the exact same time and in the same way, however problems with the measurement system cannot be completely ruled out. The pressure interface module, which is separate from the sensor and mounted inside the instrument pressure case, is not completely stable and changes in drift rates have been observed in the past, though never to this degree (Davis, pers. comm.). The Paroscientific gauges inside Hole 857D have been deployed far longer than those at the other Juan de Fuca CORKs, and it is currently unknown if this might affect performance of the gauges or their associated cardstack. In these older systems, each pressure sensor has its own internal temperature-sensitive crystal for temperature compensation of pressure. Since the temperature compensation is rolled into the reported pressure value

and not reported separately, it is almost impossible to discern if the drift of the temperature-sensitive crystal has changed over time (Davis, pers. comm.). At other CORKs, sensor issues have led to no data being recorded or in several cases, a clogged or crushed sampling line led to the pressure gauge acting as a recorder of thermal expansion and contraction in the sampling line. This produced unnaturally high recorded pressure values and a wildly erratic long-term record.

Reduction of water column height, on the other hand, is a testable hypothesis, and was checked against the Alvin submersible's depth records for the last 4 dives that downloaded pressure data from Hole 857D. The submersible also uses a Paroscientific pressure gauge to determine its depth and records depth once every ~5 seconds. This pressure gauge is not moved between overhaul periods: it was seated on the sub's starboard side at 86cm above the sub's base from early 2005 until late 2010. During each visit to 857D, Alvin landed on the CORK's ROV platform, generally for around an hour in order to download data from the logger. Following the dive, depth data for the appropriate time period were averaged and corrected for the local tidal cycle. Table 5.2 shows a cumulative depth decrease at Hole 857D observed by Alvin, which totals ~2.3m from 2005-10. Similar 'benchmark' checks are also performed at sites around Axial Seamount (Nooner and Chadwick, 2009) and provide an independent record of water depth over time at benchmark sites. The depth change recorded by Alvin shows that water column height has been reduced at Hole 857D. The Alvin data appear to corroborate the hypothesis that seafloor uplift occurred in southern Middle Valley between 2005-2010 and was recorded for the first time by a CORK. This hypothesized

uplift appears to have slowed in April 2010, with only a short period recorded by the CORK's internal logger as of its most recent download in June, 2010.

Year	Dive #	Depth Recorded by Alvin	Corrected Depth	Depth Change
2005	4155	2423.107m	2422.811m	----------
2007	4351	2422.203m	2422.006m	-0.805m
2008	4431	2421.954m	2421.757m	-0.249m
2010	4624	2420.709m	2420.524m	-1.233m
			Total:	**-2.287m**

Table 5.2. Depth values recorded during Alvin dives to Hole 857D from 2005-2010. Values were averaged over the period that the submersible sat on the ROV platform at the wellhead, then corrected for the local tidal cycle at the time. Cumulative depth change observed by Alvin is close to the loss of hydraulic head recorded by the pressure data logger in the CORK (27 kPa, or 2.7m).

2. Timing of 2005 Borehole Transients and Onset/End of Hypothesized Uplift

After removing tidal effects from the 2005 borehole signal, it was clear that the onset of the 40kPa transient followed a well documented seismic swarm in late February on the Endeavour Segment (Hooft et al., 2010). This swarm began on Northern Endeavour Ridge and propagated southward along the ridge over the course of six days, producing a borehole pressure change of -0.4kPa at 857D (Figure 5.6) as well as small increases in borehole pressure at Holes 1024C, 1026B, and 1027C on the eastern Juan de Fuca ridge flank. Earthquakes recorded were of magnitudes less than 5.0 and have been attributed to a magmatic intrusion on the northern Endeavour Segment (Hooft et al., 2010). Immediately following the small dilatational event at Hole 857D, pressure in the borehole began rising. This continued until 1300 GMT on November 19, 2005, when another earthquake swarm occurred on the West Valley propagating rift (Figure 5.7A) and was recorded by the SOSUS hydrophone array. At this time, borehole pressure increased by

0.8kPa within 1 hour (Figure 5.7B). Following this swarm, borehole pressure peaked and began to decrease while seafloor pressure also concurrently decreased. This November 19 swarm is potentially connected to the initiation of the hypothesized uplift in Middle Valley.

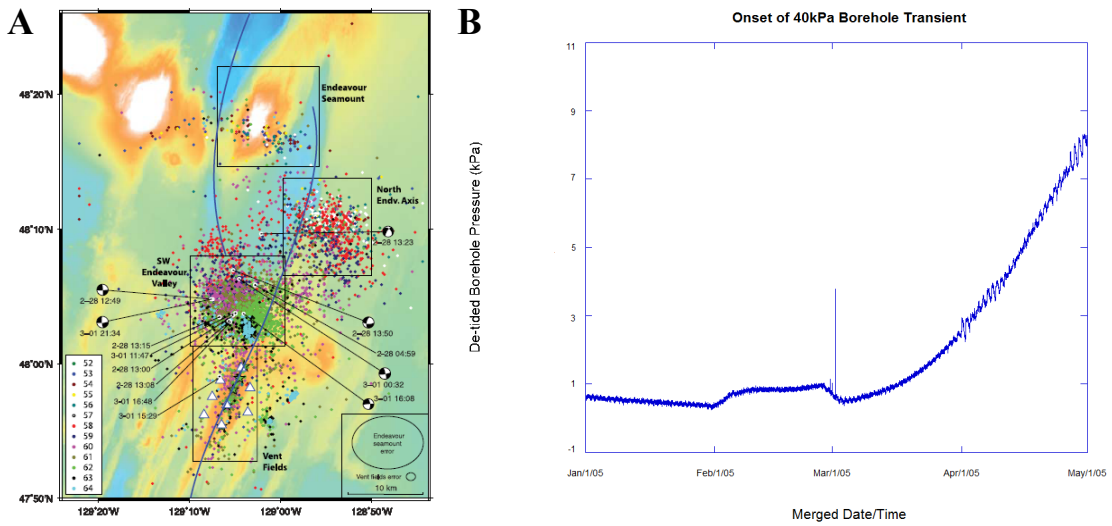

Figure 5.6. A. Map of the February, 2005 earthquake swarm that preceded the 40kPa borehole transient. From Hooft et al., 2010. **B.** 2005 borehole transient onset at Hole 857D with the effects of tides removed. See text for description.

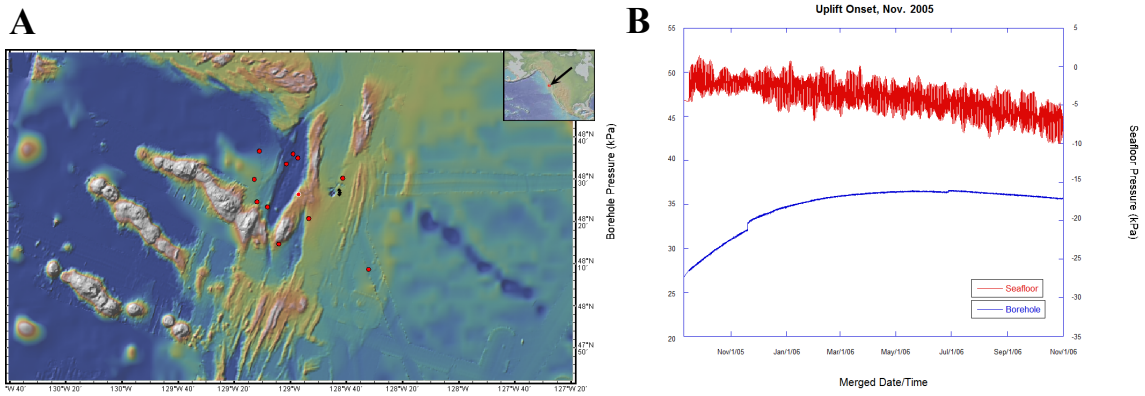

Figure 5.7. A. Map of the November 19, 2005 earthquake swarm that may have initiated seafloor uplift. Red dots indicate earthquake epicenters detected by the SOSUS network. **B.** 2005 hypothesized uplift onset at Hole 857D with the effects of tides removed. See text for description.

The rate of hypothesized uplift is constant over the subsequent 5 years and measures ~6 kPa/yr, which is equivalent to 60 cm/yr. This is four times the 15 cm/yr uplift rate recorded at Axial Seamount following its 1998 eruption (Nooner and Chadwick, 2009). Investigation of earthquake epicenter data collected in 2010 by the SOSUS hydrophone array does not reveal a clear seismic source for the end of the potential uplift period, surmised to occur in April, 2010. The end is not abrupt like the onset in 2005, therefore a seismic source may not have been required to end the hypothesized seafloor uplift, but a gradual inflation of a sill or a crustal magma lens could explain the very linear rate of pressure decrease and a gradual ending of seafloor uplift. In fact, apparent off-axis magma lenses have been observed during 3d seismic reflection studies on the fast-spreading East Pacific Rise (Canales et al., 2012) and are inferred to feed eruptions outside the direct influence of an axial magma chamber. Recalling that the initiation of this hypothesized uplift may have been related to processes in West Valley and that the sills cored at Site 857 during ODP Leg 139 had varying petrologies representing multiple magma sources, seafloor inflation by intrusion of a sill or magma lens is not an unreasonable conjecture.

3. Local Hydrothermal Response

There is a small hydrothermal field ~800m northeast of Hole 857D that has been visited several times with Alvin between 2005 and 2010 and consists of two high-temperature vent chimneys and a biologically populated diffuse flow area (Puppy Dog). Fortunately the two hydrothermal chimneys northeast of Hole 857D were both sampled prior to the hypothesized uplift onset in 2005, and several times afterwards (2007, 2008, and 2010) (Figure 5.8). The chimneys initially maintained a stable fluid temperature of ~270°C

through 2008, however in 2010 when we returned to the chimneys one had ceased venting and was covered with benthic fauna, while the other (which had been toppled for a temperature measurement in 2008) was reduced from a meter to ~10cm in height, appeared to consist entirely of anhydrite, and was venting ~180°C fluids. On a subsequent cruise in 2010, high-temperature vents to the north of Hole 857D near Site 858 were also observed to have shut down or were venting much less vigorously than previously observed (Girguis, pers. comm.). Based on the assumed connectivity between the formation at Hole 857D and the local hydrothermal system, determined thermally during ODP Leg 139 (Shipboard Scientific Party, 1992a), it is possible that the changes in the character of local vent sites seen in 2010 are related to the end of the apparent seafloor uplift. The lower venting fluid temperatures and general decline of previously robust vent fields suggest the loss of a heat source, the closure of fluid pathways that supply the vent fields, or a combination of both. In the case of the vents near Hole 857D, the almost 100ºC fluid temperature drop in a region with few local fluid recharge zones points strongly to the loss of a heat source. If the hypothesized seafloor uplift was tied to magmatic intrusion into the crust in southern Middle Valley, then the heat from that source could have fed the small vent field. Then as the heat source waned as the intrusion cooled, venting fluids would in turn have cooled: a process observed at the 9ºN Integrated Study Site on the East Pacific Rise (eg. Fornari et al., 1998).

5.5 Discussion/Summary

The 2005-11 pressure record from the CORK at Hole 857D is unlike any previously observed signal from a subseafloor observatory installed at or near a mid-ocean ridge

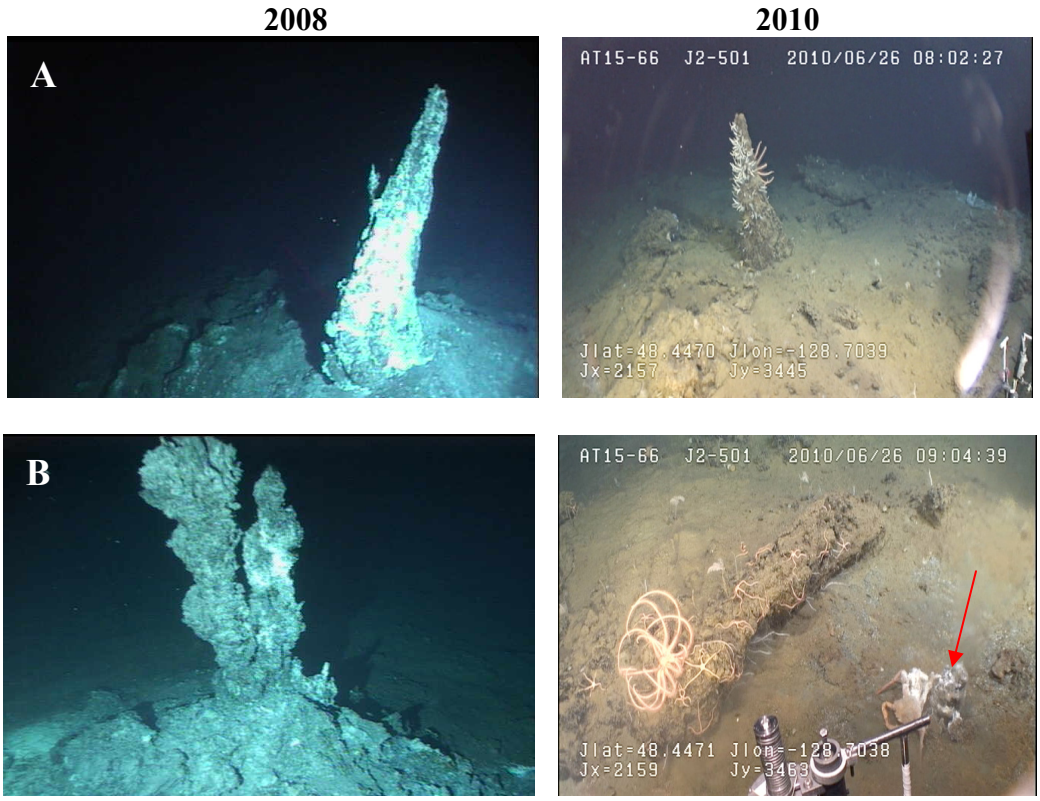

Figure 5.8. Comparison of 2 chimneys near Hole 857D from 2008 to 2010. Chimney A has shut down completely while Chimney B is drastically reduced in size (indicated by arrow) and venting at a much cooler temperature.

crest. Prior to 2005, the largest formation pressure transient at Hole 857D was in 2001, attributed to a large earthquake swarm within Middle Valley that caused a ~15kPa drop in formation pressure (Davis et al., 2004). It is important to note that the 2001 earthquake swarm, which lasted for a period of 21 days and consisted of nearly 14,000 events, was the largest, singular earthquake swarm on the Juan de Fuca Ridge recorded by the SOSUS hydrophone array (Dziak, pers. comm.). Immediately following the swarm, a response cruise did investigate Middle Valley in search of new hydrothermal plumes, however little evidence was found of any effects on the local hydrothermal system and it was concluded that any void space created by dilatation filled with water and not magma (Davis et al., 2004). Current insight into the eruptive frequency of mid-

ocean ridges places them on a decadal scale (eg. Perfit and Chadwick, 1998), and prior to the latest eruption at Axial Volcano in 2011, Chadwick et al. (2006) were able to predict its occurrence with confidence, based on their seafloor benchmark measurements in the area. If a decadal eruptive cycle is indeed controlling the Middle Valley/West Valley segment, then the region may be due for another significant seismic event within the next several years, potentially heralded by the presence of hypothesized seafloor uplift and stark changes in the local hydrothermal system at the southern end of the rift valley.

One significant difference between previous borehole transients attributed to seismicity and the Hole 857D 2005 event is that, following a rapid pressure change due to dilatation or compression, pressure in the formation tends to slowly return to its pre-transient state. This is not the case here if the seafloor pressure history is correct; following the initial ~40 kPa increase, differential formation pressure does not decay and actually continues to rise in concert with seafloor pressure during the period of hypothesized uplift (Figure 5.9). This is unlike anything previously observed in a subseafloor pressure record and certainly indicates a different source than previous transient events in CORK pressure records have alluded to. A short lived seismic source yields quick spikes or drops in differential pressure, not the extended period of pressure elevation observed here.

Looking back to the March 2005 earthquakes that started the initial rise in formation pressure at Hole 857D, and recalling that they also initially caused slightly elevated pressures in the Juan de Fuca ridge flank CORKs, it begs the question of looking for complementary pressure transients during the period of uplift in the ridge flank pressure records. Hole 1024C, the ridge flank CORK closest to the crest and most affected by the

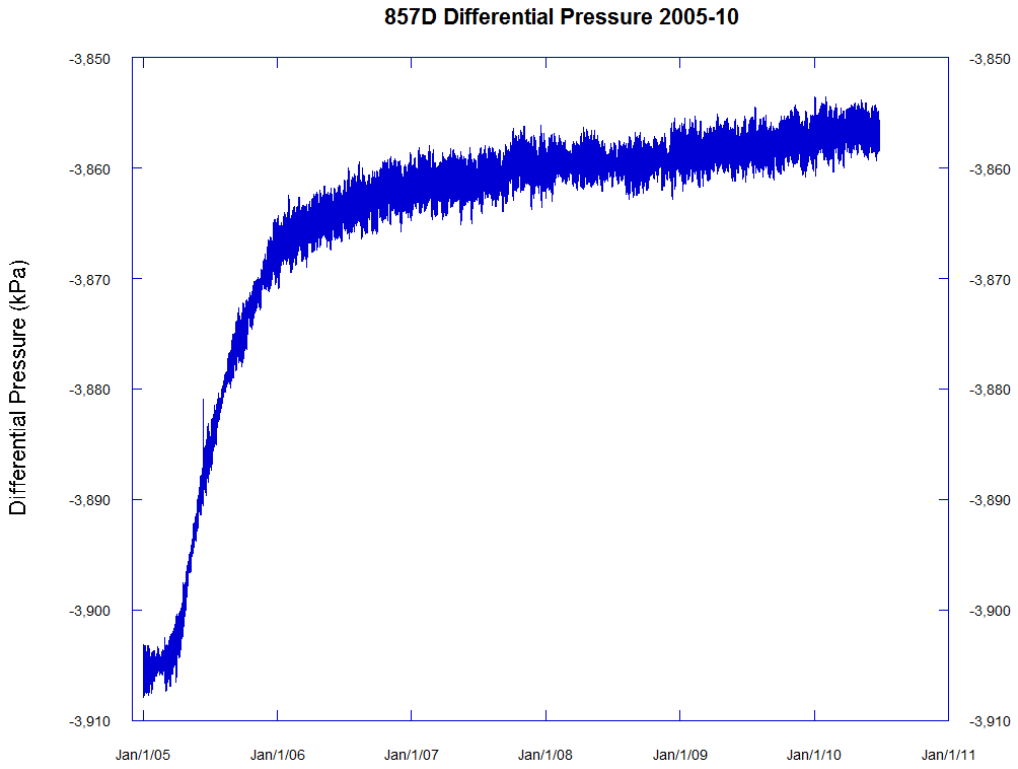

Figure 5.9. Differential pressure from Hole 857D, 2005-2010, calculated by subtracting seafloor pressure from formation pressure. Note that this calculation was done with data from which tidal effects had been removed.

March 2005 swarm, however does not show any clear response to either the November 2005 West Valley swarm, nor to the 4.5 years of hypothesized seafloor uplift that followed. One must therefore conclude that whatever process affected Middle Valley during that time, its field of influence did not extend beyond the West Valley-Middle Valley region, unlike the larger (albeit short-lived) regional influence by earthquake swarms on the northern Juan de Fuca Ridge.

Further data are required in order to quantify any areal extent of the hypothesized uplift and its effect on Middle Valley's hydrothermal system. Fine-scale mapping of the seafloor around Hole 857D and the small hydrothermal field nearby would provide clarity as to whether the uplift signal observed at 857D is 1) real and/or 2) represents the

maximum vertical displacement in the area, or if deformation has been more significant elsewhere. A new set of Ocean Bottom seismometers and hydrophones was deployed on Juan de Fuca in Fall 2011, some of which are located inside Middle Valley, in a continued effort to monitor any regional seismicity. If the decadal-scale mid-ocean ridge eruptive cycle applies to processes here, then there is a good chance that another large earthquake swarm, not unlike the one observed in 2001, could sweep through Middle Valley in the immediate future. If we can observe this, the accumulated data could be vital for understanding eruptive processes at sedimented ridges worldwide and how they compare to processes at unsedimented ridges, such as the intensely studied 9ºN segment of the East Pacific Rise.

It is possible that seafloor uplift occurred in Middle Valley between 2005 and 2010, based both on observations recorded by the downhole logger at Hole 857D, as well as benchmark checks made by the DSV Alvin during routine service dives. Using the data presented in this chapter alone, it is difficult to pinpoint accurately the geologic agent of Middle Valley's ~4.5 year seafloor uplift, although several tentative ideas have been presented. A potential uplift source will be constrained and discussed thoroughly in the following chapter.

CHAPTER SIX:

MODELING THE POTENTIAL SEAFLOOR UPLIFT AT 857D

6.1 Motivation

In chapter 5, the potential for seafloor uplift in southern Middle Valley between 2005 and 2010 was established using pressure data from the CORK at Hole 857D and depth records from the Alvin submersible. Assuming these data are correct, this chapter will use numerical modeling to approximate the potential uplift, in an effort to quantify and constrain the geologic process(es) causing it. However, the data available do place some limitations on what models can be used: since we only have data for one point on the seafloor, we do not know if the hypothetical uplift is the center of uplift or along the flank of a larger uplifted area. The lack of bathymetric maps of sufficiently high-resolution in this region, both before and after uplift, also limits the scope of any models we might employ, as we cannot be sure of the surface shape and lateral extent of the uplifted region. It is critical to note that seafloor uplift of this magnitude/rate has not been observed by a CORK previously, thus any modeled result can only be compared to other submerged, sustained magmatic systems, such as Axial Volcano (Nooner and Chadwick, 2009), or subaerial volcanic systems such as Long Valley Caldera (eg. Dixon et al., 1993) and Sierra Negra (eg. Chadwick et al., 2006a).

6.2 The Mogi Model

To model the source of an uplifted surface, be it subaerial or submarine, it is important to know the shape and lateral extent of the surface, as well as vertical and horizontal displacements in time. Since our knowledge of the lateral extent of uplift in Middle

Valley is extremely limited, we must begin by considering a simple model to approximate the observed vertical change. For example, we lack sufficient data at this time to use a model such as Okada's for approximating a rectangular dislocation (sill or dike) in an elastic half space (Okada, 1985), as it requires knowledge of both lateral and vertical displacements. Despite our limited data, we can incorporate additional data from other studies to constrain a magma source and depth, which could potentially be used to model a sill. However, we will first consider the expansion (ΔV) of a point-source within an elastic half space (a simple spherical magma chamber) beneath Middle Valley as a source of displacement, which can be explained by 2 equations in terms of change in height U_z, and change in horizontal distance U_r (Mogi, 1958):

(1) $$U_z = \frac{3\Delta V d}{4\pi(d^2 + r^2)^{1.5}}$$

(2) $$U_r = \frac{3\Delta V r}{4\pi(d^2 + r^2)^{1.5}}$$

where ΔV is the change in volume (m^3) of a spherical magma chamber, d is the depth to the center of the magma chamber, and r is radial distance from the surface point above the center of the magma chamber (Figure 6.1). The equation for vertical displacement contains 4 variable parameters (r, d, ΔV, and U_z), thus we must constrain 3 in order to determine the parameter of interest (here, d). In order to produce the magnitude of vertical displacement observed in Middle Valley, at what depth would the center of point source expansion occur? Does this modeled magma chamber fit within the geologic setting and with accepted magma chamber depths for the region?

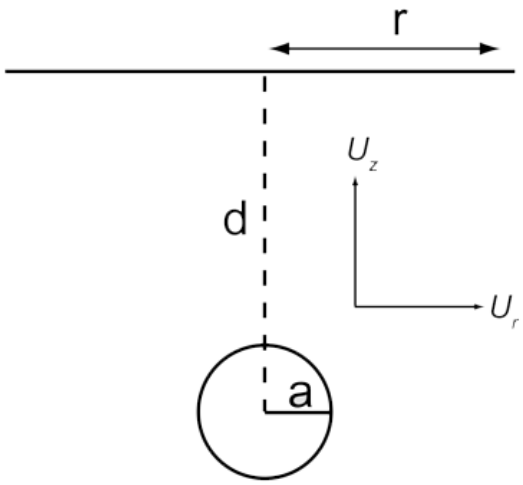

Figure 6.1. Simple diagram of a point source within an elastic half-space, as utilized in the Mogi model (Equations 1 and 2). Parameters are defined in the text above, and $d >> a$, the radius of the magma chamber.

6.3 Applying the Mogi Model to Middle Valley: Parameter Constraints

Since we currently have only one data point of observed vertical change on our unconstrained uplifted surface, initially Hole 857D will be considered as centered over the modeled magma chamber ($r = 0$). Also as a result of our limited data, we are forced to make some assumptions regarding constraints on the parameter ΔV; these constraints are based on observed injection rates at other locations with a sustained magmatic source. For example, the estimated sustained injection rate into Axial Volcano's shallow magma chamber between 2003 and 2007 was ~0.0075 km^3/annum (Nooner and Chadwick, 2009), while the subaerial system at Long Valley Caldera had an estimated injection rate of 0.020 - 0.034 km^3/annum, dependent on the assumed magma chamber depth, for the 3.3 year period of 1988-1992 (Dixon et al., 1993). The volumes considered for this model interpretation and their corresponding magma chamber depths are outlined in Table 6.1 along with each system's uplift rate, with Middle Valley's rate noted for comparison. Furthermore, since the uplift rate in Middle Valley is approximately 4 times the uplift

rate of Axial Volcano, we will constrain our injection volume between that of Axial's average rate and 4 times its average rate for the purposes of this study. This range is similar to the injection rates observed at Sierra Negra and Long Valley. Finally, we will force U_z = 60 cm/yr in accordance with the observed uplift rate at 857D.

Parameters from Other Volcanic Systems and Middle Valley

System	Depth to Magma Chamber (d), km	Injection Rate (km^3/annum)	Observed Uplift Rate (cm/annum)
Axial Volcano, JdF, 2003-2007[1]	2.2 - 3.5	0.0075	12
Long Valley Caldera Resurgent Dome, CA, 1988-1992[2]	7 - 9	0.020 - 0.034	2.4 - 2.7
Sierra Negra Volcano, Galapagos, 2004-2005[3]	2.2	0.017	220
Middle Valley, JdF, 2005-2010	?	?	60

Table 6.1. Parameters used to constrain the Mogi model for the purpose of this work. Uplift histories for Long Valley and Sierra Negra were determined by GPS and space geodesy techniques, while Axial Volcano's was determined using seafloor benchmarks around and inside the caldera. Note that while both Axial's and Long Valley's injections were into a magma chamber, Sierra Negra's was sill emplacement. However, it is a subaerial volcanic system that has been modeled previously with the Mogi equation, thus its inclusion.
[1] (Nooner and Chadwick, 2009); [2] (Dixon et al., 1993); [3] (Chadwick et al., 2006).

6.4 Model Results

By using equation (1) given above and constraining the parameters as noted previously; we obtain a range of magma chamber depths. Table 6.2 shows the range of magma injection rates used along with the resultant magma chamber depths, which varied between 1.7 and 3.6 km. The modeled results from Middle Valley were then plotted along with other geological sites for comparison (Figure 6.2).

Mogi Model Applied to Middle Valley

Injected volume (ΔV), km^3/annum	Depth (d), km	U_z, m/annum
0.0075	1.727	0.60
0.0125	2.230	0.60
0.0175	2.638	0.60
0.0225	2.990	0.60
0.0275	3.306	0.60
0.0325	3.595	0.60

Table 6.2. Resulting magma chamber depths generated with the Mogi model by using equation (1) for a range of potential magma injection volumes beneath Middle Valley.

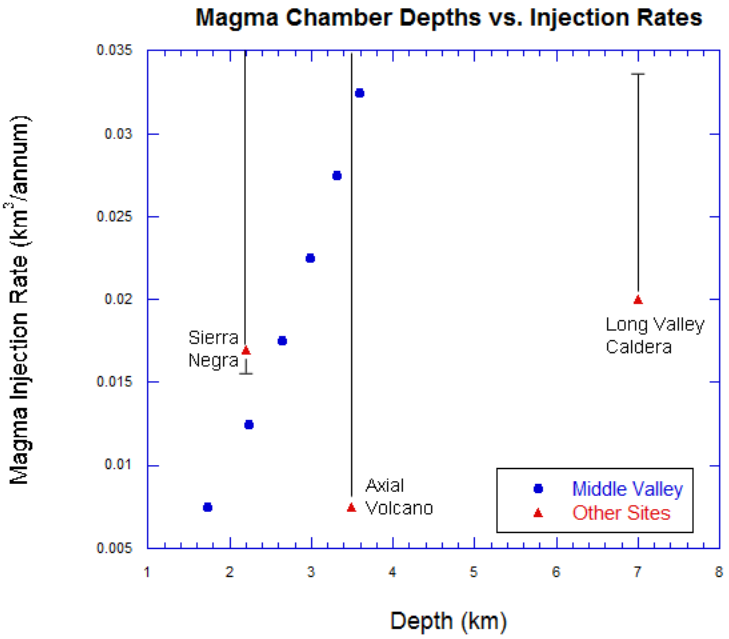

Figure 6.2. Modeled magma chamber depths for Middle Valley plotted against injection rate. Other sites previously mentioned are included for comparison. Maximum injection rate at Sierra Negra was 0.064 km^3/annum immediately prior to the 2005 eruption (Chadwick et al., 2006a). Axial Volcano's injection rate reached 0.14 km^3/annum for one month following the 1998 eruption, then decayed to 0.036 km^3/annum for the following 6 months before settling to 0.0075 km^3/annum for the remainder of the uplift period (Nooner and Chadwick, 2009).

6.5 Interpretation

It is clear from the results of modeling uplift rates in Middle Valley that a variety of magma chamber depths can produce uplift of the magnitude observed at Hole 857D. Due to the tradeoff between depth and source volume, shallower magma chambers require

smaller volumetric inputs to generate the same uplift as a deeper magma chamber with a larger injection volume. If we consider what has been observed about both sustained subaerial and submarine volcanic systems, we can make a first attempt at constraining the potential magma chamber depth in Middle Valley.

1. Magma Chamber Depth: Middle Valley vs. Axial Seamount

If we assume that the injection rate in Middle Valley is up to four times Axial's injection rate, then in order to generate the observed uplift the magma chamber depth for the largest injection rate is between 3.3 and 3.6 km^3/annum. The magma chamber beneath Axial Volcano has been imaged using seismic tomography and appears to vary in depth between 2.2 and 3.5 km, with the shallowest portion located at the intersection of the extension of the Heckle Seamount chain and the Endeavour segment (Carbotte et al., 2008). So our modeled magma chamber fits geologically with what has been modeled at Axial, which is unsurprising since our injection rate constraints were based mainly on those of the same system. How does our modeled magma chamber compare geologically to other systems and the Juan de Fuca Ridge as a whole?

2. Magma Chamber Depth: Middle Valley vs. Other Volcanic Systems

The subaerial Long Valley Caldera has an estimated magma chamber depth of 7-9 km, which is shallow for a continental magmatic system, but entirely too deep for an oceanic spreading center where the total crustal thickness is 4-6 km. Additionally, the subaerial Sierra Negra volcanic system in the Galapagos Islands has a magma sill depth around 2.2 km that fed its 2005 eruption (Chadwick et al, 2006). So our modeled magma chamber is

a closer geologic fit for a Sierra Negra-like subaerial system, as opposed to Long Valley Caldera whose magma chamber is far too deep to be comparable to a ridge crest system.

3. Magma Chamber Depth: Middle Valley vs. the Juan de Fuca Ridge

Since the northern Juan de Fuca Ridge spreads at a rate of ~6 cm/yr, it is unlikely we would observe a very shallow magma body depth of 1-1.6 km as observed on the fast-spreading 9ºN segment of the East Pacific Rise (eg. Detrick et al., 1987). In fact, a discontinuous magma lens has been observed beneath the Endeavour segment at a depth range of 2.2 - 3.3 km, with the shallowest section located beneath the Main Endeavour vent field (Van Ark et al., 2007). North of the Endeavour segment, in West Valley, insufficient seismic data are available to determine magma chamber depth, let alone its presence, although petrologic studies of zero-age rocks dredged from this area show compositional heterogeneity potentially caused by mixing of mantle source domains or mixing within the magma chamber (Van Wagoner and Leybourne, 1991). Despite the lack of knowledge about West Valley, our modeled magma chamber depths for the most part fit with the 2.2 - 3.3 km melt lens depth range observed on the Endeavour Segment.

4. Observed Seismicity: Middle Valley vs. Axial Seamount

Another important point to consider is whether or not a magma chamber expansion beneath Middle Valley would produce observable seismicity for a magmatic inflation based on the constraints previously described. Axial Seamount experienced large seismic swarms in 1998 (>9000 events) that preceded seafloor volcanic eruptions and deflation, and were observed by both the SOSUS network and ocean bottom hydrophones (Dziak and Fox, 1999). Again in 2011, the eruption at Axial was preceded by a seismic swarm

(hundreds of events, although only a few were detected by SOSUS) however seismicity between eruptions, and coincidentally during magmatic post-eruptive inflation of ~3m, was minimal (Chadwick et al., 2006). Middle Valley was affected in early 2005 by a large earthquake swarm on the Endeavour segment (Hooft et al., 2010) and a small swarm 6 months later in West Valley as discussed in Chapter 5, and then was seismically quiet until a small swarm in May 2009 was recorded by SOSUS and land-based seismometers, consisting of ~21 events with magnitudes of ~3 and located to the southwest of southern Middle Valley (Figure 6.3) (Dziak, pers. comm.). Although these earthquakes were located quite close to Hole 857D, fluid pressures in the borehole remained unaffected, and the overall linear trend continued without interruption for a year afterwards. Based on patterns of seismicity, Axial Seamount and Middle Valley are similar in that large local seismic swarms are generally absent during periods of long-term inflation that are on the same total meter-scale. Although the 2009 swarm located southwest of Middle Valley did not perturb fluid pressure, it is difficult to say if this swarm had any structural or magmatic implications that might have affected the ongoing process, as uplift halted roughly a year later in early 2010.

6.6 Discussion

1. Uplift Elsewhere in Middle Valley

With the caveats that this model assumes that the data are verified and reflects only one data point on the seafloor (which we have assumed represents the center of maximum uplift), we have been able to constrain a potential magmatic source of depth ~1.7 to ~3.6 km using a ΔV between 0.0075 and 0.0325 km^3/annum, producing a 60 cm/yr uplift rate.

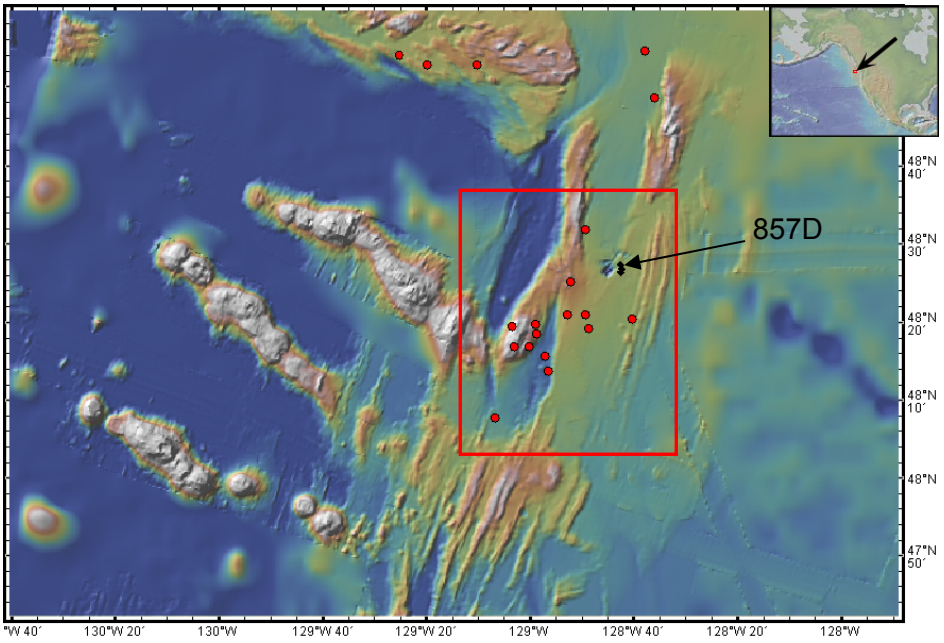

Figure 6.3. Earthquakes detected by SOSUS and land-based seismometers in May 2009. The box bounds earthquakes closest to Hole 857D that did not affect the overall linear trend in borehole or seafloor fluid pressure data.

However, does this theoretical source describe deformation on the seafloor away from the CORK? While we do not have fine scale bathymetric maps of this region, we do have our continued observations and navigational data at the vent site ~800m northeast of Hole 857D, but they are not nearly as precise as the Alvin records used to substantiate the uplift at Hole 857D, as the submersible does not necessarily sit in the same place during each visit to the chimneys. If we calculate U_r (Equation 2) for a point 800 m (here, representing the vent site) from the point above our theoretical magma chamber, we obtain centimeter scale horizontal relative motions per year which, even integrated over 2005-2010, would be impossible to resolve in navigational data. Additionally, calculating average depths for each visit (2005, 2007, and 2008) to the chimneys with Alvin does not reveal any significant depth change from 2005 to 2007, and only a small depth change between 2007 and 2008 (Table 6.3); although it is unclear if this is due to

the lack of a permanent benchmark or simply the absence of uplift at this location. We will begin by assuming that little to no uplift has occurred ~800m away from Hole 857D.

Year	Dive #	Depth Recorded by Alvin	Corrected Depth	Depth Change
2005	4155	2414.845 m	2414.475 m	----------
2007	4351	2415.213 m	2414.423 m	-0.052 m
2008	4431	2413.466 m	2413.865 m	-0.558 m
			Total:	**-0.610 m**

Table 6.3. Alvin depth data recorded at the high temperature chimneys ~800m northeast of Hole 857D. These data have been averaged and corrected in the same manner as those shown in Chapter 1, however in this case there is no benchmark to provide a consistent location from year to year. Note that there was only a ~60cm total depth change over the 3 years recorded and unfortunately Alvin did not visit the chimneys during its 2010 dive.

With this assumption and the model we have previously generated for a spherical magmatic source beneath Middle Valley in mind, we can reconcile theoretical uplift values generated by the Mogi model with geologic evidence. Using the magma chamber depths and their accompanying magma injection volumes obtained from the model, we can use Mogi's equation (1) to approximate the annual uplift for the vent site. The results of this calculation are in Table 6.4 and clearly show that for these theoretical magma chambers, a site ~800m away would have experienced a significant amount of uplift over the 4.5 years of uplift observed at Hole 857D. Our depth data from the vent site do not show a consistent uplift response since uplift onset; only between 2007 and 2008 was there any significant amount of change (~55 cm) that is of the magnitude generated by this model (Figure 6.4).

Modeled Uplift at Vents Northeast of 857D

Magma Injection Volume (km^3/a)	Magma Chamber Depth (km)	Uplift Rate at Vent Site (m/a)
0.0075	1.727	0.4485
0.0125	2.230	0.5004
0.0175	2.638	0.5261
0.0225	2.990	0.5416
0.0275	3.306	0.5515
0.0325	3.595	0.5584

Table 6.4. Results generated with the Mogi equation (1) for the vent site located ~800m from the CORK at Hole 857D.

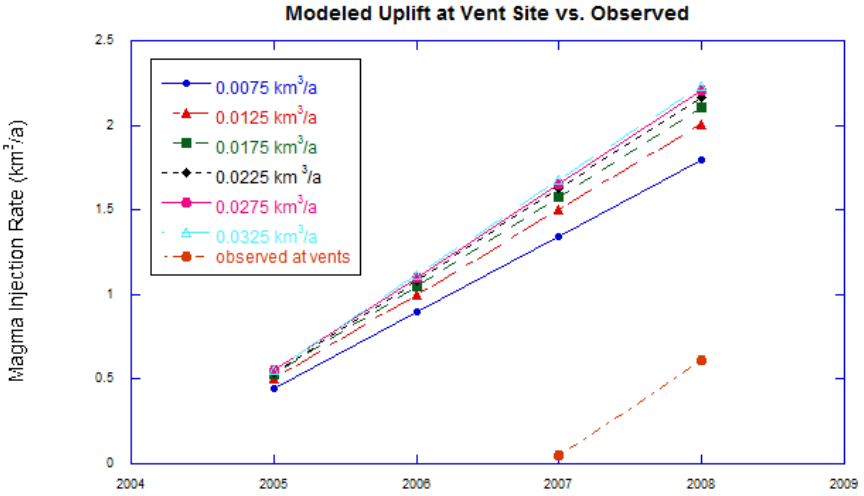

Figure 6.4. Theoretical uplift at the vent site through time, assuming a spherical magma chamber centered beneath Hole 857D, based on values from Table 6.4, compared to the actual, smaller uplift observed by *Alvin* at the same site.

If however, we assume that the observed total depth change at the vents is real, and that it is coincident with 2m of uplift at Hole 857D, we can use the Mogi equation (1) twice to solve for a magma chamber depth that would produce such an uplift pattern. Doing so yields a value of 2.164 km for magma chamber depth, which is within the range previously identified as geologically feasible for Juan de Fuca. Thus, if the depth change observed at the vents is to be believed, and the source is at 2.164 km depth, the total injection volume would be ~0.015 km^3 over the period of 2005-2008, or ~0.005 km^3/annum.

2. Co-Seismic Strain of the Uplift-Initiating Event

In addition to contemplating uplift away from Hole 857D, we can also consider the seismic swarm in West Valley that coincides with the 0.8 kPa increase in borehole pressure that was established in Chapter 1 as the event that may have initiated uplift. Does an elastic pore pressure response of this magnitude result from a change in volumetric strain that is expected and/or reasonable for a spreading event along the Juan de Fuca ridge crest?

I. Calculating Volumetric Strain from Pore Pressure Change

Following the observation of pressure transients that occurred contemporaneously with earthquake events on the Endeavour segment in 1999, Davis et al. (2001) proposed that the transients were the result of initial co-seismic elastic strain followed by hydraulic diffusion in the formation as it returned to its original state. The initial sharp change in pressure is assumed to be rapid relative to hydraulic diffusion (ie. Darcy flow does not occur), which allows for porefluid pressure change to be expressed as a function of the physical properties of the formation. Under this assumption, Davis et al. (2001) derived that under undrained conditions volumetric strain θ is related to effective pressure P by:

(3) $$\theta = \frac{1-\alpha\beta}{\beta K} \cdot P$$

where: $$\alpha = 1 - \frac{K}{K_s}$$

and: $$\beta = \frac{1}{1 + n(K / K_f)}$$

where parameter β is the 3-dimensional loading efficiency of the formation, n is porosity, and K, K_f, and K_s are the bulk moduli of the matrix frame, the fluid, and the solid portions of the matrix. Using these equations with the appropriate parameters, we can calculate the compressional or dilatational volumetric strain that occurred during a pressure transient observed at Hole 857D. For the purposes of this work, the parameter values used are as follows.

K	14.7 GPa
K_f	0.75 GPa
K_s	50 GPa
β	0.20

By using these equations relating pore pressure change to co-seismic volumetric strain, we can calculate the strain necessary to generate a 0.8 kPa borehole pressure increase. Using equation (3), compressional volumetric strain experienced by the borehole was 2.34×10^{-7}, which is the same order of magnitude as the upper end of the range of co-seismic strain calculated for the 1999 Endeavour segment earthquake swarm that caused borehole pressure transients at several Juan de Fuca CORKs on the ridge flank and in Middle Valley (Davis et al., 2001). That swarm was determined to have been related to a spreading event with ~12 cm dilatation. No extrusive volcanism was associated with the event, but magma injection cannot be excluded as a possible source. In the case of the November 2005 swarm, the formation at Hole 857D does not exhibit diffusive drainage following the initial elastic response to the strain change (indeed borehole pressure continued to rise), indicating that we are not looking at a simple borehole pore pressure

response to an earthquake swarm. Clearly geologic processes resulting from the 2005 West Valley swarm differ from the 1999 Endeavour swarm, in that the pore pressure responses are markedly different.

3. Magma Source

An additional point to consider in Middle Valley's geologic context is the petrologic composition of the basalts observed in Hole 857D. The sill chemistries have multiple magma sources: one is a typical N-MORB, another is a transitional T-MORB (dominating the section recovered), and the third source is a mix of the two endmember compositions (Stakes and Franklin, 1994). The fact that Middle Valley has been influenced by multiple magma sources in its history indicates a complexity similar to Axial Volcano, which is also influenced by multiple sources (Nooner and Chadwick, 2009) due to its proximity to the Heckle Seamount chain. However, unlike Axial, the rate of uplift observed at Hole 857D was constant over its duration, implying a constant rate of ΔV. Axial on the other hand, initially had a higher ΔV, which decreased significantly after six months and may have been the result of an initial influx of magma from shallow satellite magma bodies (Nooner and Chadwick, 2009). If we assume this is correct, any uplift-producing magma chamber in Middle Valley is less likely to have received sporadic magmatic input from multiple sources due to its constant rate over 4.5 years, although it may be a satellite magma body itself compared to a magma chamber beneath the axis of spreading in West Valley, which also exhibits compositional heterogeneity as mentioned previously. However, the observed crustal structure at Hole 857D is sill-dominated, implying that the area is subjected to lateral sill emplacement that has tapped multiple sources.

4. Sill Intrusion

Considering the absence of uplift of the magnitude predicted by the Mogi model for the vent site and the presence of a sill-dominated basement section observed at Site 857, we must also consider the possibility of lateral sill intrusion as a source of the observed uplift. Seismic studies during ODP Leg 139 were able to define several sills that run parallel to the extensional faults in the center of Middle Valley (Figure 6.5) and approach dimensions of 7 km long and 1 km wide (Rohr and Schmidt, 1994). These features are defined as sills rather than flows or dikes based upon the seismic sections taken across Middle Valley, which have reflector trains that are indicative of sill-sediment sequences, and because no lava flows are exposed on top of the sediment section (Davis and Fisher, 1994; Rohr and Schmidt, 1994). Based on basement structure, if we once again consider Hole 857D as centered over a theoretical sill that grows to 3 m thickness (to reflect the observed uplift) with similar areal dimensions to the other sills defined, is such a sill possible volcanically and/or thermally? Can we use such a sill to explain the delayed, small magnitude uplift observed at the vent site?

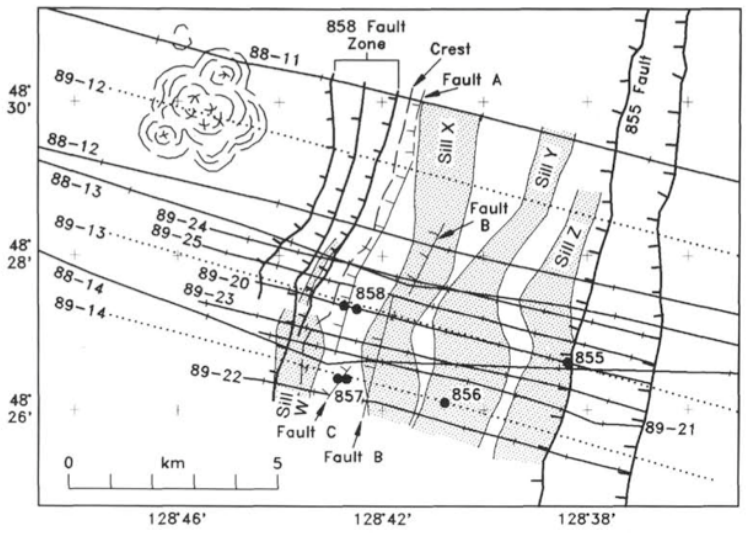

Figure 6.5. Middle Valley's identified sills. See text for discussion. From Rohr and Schmidt (1994).

I. Sill Volcanics and the West Valley Swarm

Downhole logging of Hole 857D during Leg 139 revealed that 26 individual basaltic sills with thicknesses ranging from 1 to 25 meters were penetrated by drilling (Langseth and Becker, 1994). As mentioned previously, Site 857 sill basalt chemistries vary between N-MORB and T-MORB compositions. If we are considering sill intrusion as a source of uplift, can the volcanics of the region explain this? Consider that the uplift-inducing November, 2005 earthquake swarm in West Valley produced a co-seismic strain comparable to the 1999 Endeavour swarm. The West Valley swarm may have included a dike injection from a magmatic source that also fed the sill intruding beneath Hole 857D. Clearly Middle Valley has experienced sill intrusion in its geologic history, sometimes by basalts of similar composition to those found in West Valley (Stakes and Franklin, 1994). Also consider that off-axis (4-8 km) melt lenses are observed along segments of mid-ocean ridges, most recently on the 9ºN segment of the EPR (eg. Canales et al., 2012) and may represent melt migration pathways that promote mixing, producing differing basalt chemistries, a feature observed in the sill-sediment complex in Hole 857D. The timing of seismicity in West Valley and Middle Valley's proclivity for sill intrusion certainly indicates that present-day sill intrusion is volcanically possible in Middle Valley, based on both geologic history and chemistry of existing sills.

II. Sill Thermal History

The more critical caveat to considering sill intrusion as our uplift source is the conductive cooling rate of the intruded sill. What is the cooling time and/or rate for a 3 m thick sill if we assume a 1:1 sill thickness to uplift ratio? Is this time reasonable considering the length of uplift? Let us consider the simplified equation for the cooling of a sill, recalling

that a magma body will solidify from the edges towards the center (and will be completely solid at time *t*), assuming no internal convection or release of latent heat of crystallization:

(4) $$t \approx \frac{b^2}{\kappa}$$

Where *b* is the vertical half dimension of the sill and κ is thermal diffusivity, defined as the thermal conductivity divided by density and specific heat. We will assume a 3m thick sill with a lateral extent similar to the sills previously identified and a thermal diffusivity of 8.3 x 10^{-7} m^2/s, based on a bulk density of 2.25 g/cm^3, a grain conductivity of ~3W/m K (Villinger et al., 1994), and a specific heat of 1.6 kJ/kg for Site 857 basalt. This yields a rough cooling time of 750 hours (31.25 days), which does not concur with a 4.5 year uplift event. Refining solidification time further, if we consider the previous sill cooling equation and include the release of latent heat of crystallization, the solidification time is:

(5) $$t_s = \frac{b^2}{4\kappa\lambda^2}$$

where λ is a dimensionless term and:

$$\frac{L\sqrt{\pi}}{c(T_m - T_0)} = \frac{e^{-\lambda^2}}{\lambda(1 + erf\lambda)}$$

Where *L* is latent heat of crystallization, T_m is magma emplacement temperature, T_0 is the initial temperature of country rock, and *c* is specific heat (Turcotte and Schubert, 2002). We will assume a latent heat of 400 kJ/kg, a specific heat of 1.6 kJ/kg K, an emplacement temperature of 1600K, and a country rock temperature of 280ºC (553K) for the intruded sill, which yields a λ of ~0.765. Using equation (5) we then calculate a

solidification time of 320 hours (13.3 days) for a 3 m thick sill. This is a much shorter timescale than the 4.5 year uplift period observed, and the mismatch between the two is large enough to exclude simple sill emplacement as a cause of the observed uplift. Note that the sill cooling equations do not consider the heat supplied by lateral flow within the sill, nor the insulating effects of the sediment, both of which will tend to extend the cooling history of the sill. Emplacement rate or sill accretion velocity is also ignored, defined here as the sill thickness divided by the time interval between two sill injections (Annen, 2011). Additionally the boundary condition of a constant temperature in country rock necessitates that permeability of the material must be high, while in reality it is likely low. Cooling is likely conductive and thus an injected sill would be expected to take longer for complete cooling. Were the sill injected at a greater depth where the country rock is at a higher temperature, this would also extend the cooling time.

If we instead use our observed uplift period of 4.5 years as our solidification time and the same constants as above, we can calculate the thickness of a theoretical intruded sill as ~16.6m, which is well within the range of sill thicknesses drilled during Leg 139. We must therefore consider that if a cooling sill was responsible for the observed uplift, that 857D was not the locus of maximum uplift due to that sill, still assuming a 1:1 ratio of sill thickness to observed uplift. In this case, considering the minimal uplift observed at the vent sites to the northeast, one might expect larger magnitude uplift to the west of 857D closer to West Valley, which would make sense geologically if the sill's source is the same magma source that feeds West Valley. However our lack of baseline high-accuracy bathymetry (0.1 m scale) for the area prevents us from confirming or refuting this. Thus we cannot completely exclude sill intrusion as a possible uplift source.

6.7 Summary

Using the Mogi (1958) equation, we have made a first attempt at constraining the properties of a magma chamber that would produce the magnitude of uplift recorded by the CORK at Hole 857D, having made the assumption that the data are verified. The modeled magma chamber depths are comparable to those observed in seismic tomography studies of both the Endeavour segment as well as Axial Volcano. However our assumptions and small dataset limit the confidence with which the results from this model can be accepted. Latest available data from the Hole 857D high-resolution data logger (June 2010 through September 2012) suggest that the uplift signal recorded by the downhole logger may in fact be an artifact of gauge drift and/or failure, however the source of this problem with the seafloor pressure gauge is unknown. Linear gauge failure of this kind has not been observed previously in CORK data records. Were it not for the high-resolution logger we would not have known about this issue, as the Alvin data do appear to corroborate the seafloor depth change (though we know nothing about the drift of the Alvin gauge). It is clear that we must strive to collect data from independent sources in order to verify CORK pressure data, though this will not always possible due to the money and time necessary for deploying backup logger systems or bottom pressure recorders on the seafloor.

If in fact we are looking at an artifact in the seafloor pressure data, then little to no vertical uplift may have actually occurred. Unfortunately, that makes the presence of an injected magma body improbable. This then brings into question what caused the dramatic changes in venting in Middle Valley between 2008 and 2010. In this case, a

shutdown of venting might be related to the gradually decreasing formation pressure over time, the 2009 seismic swarm, or some other unknown process entirely.

CHAPTER SEVEN:

1996 CROSS-HOLE EXPERIMENT BETWEEN HOLES 857D AND 858G

7.1 Experimental Description

In 1996, during the replacement of the CORKs in Holes 857D and 858G during ODP Leg 169, drilling operations were ordered such that an experiment be conducted to test the hydraulic connectivity of basement between Holes 857D and 858G. First, the CORK in Hole 858G was fully replaced. Then, while replacing the damaged CORK in Hole 857D, seawater was circulated down to the high permeability zone previously observed at 610 mbsf with the purpose of creating a pressure transient that would propagate to Hole 858G, and which would be recorded by the CORK (Figure 7.1). The nature and magnitude of the deviation in borehole pressure ideally could then be used to make inferences about the permeability of basement between Holes 858G and 857D.

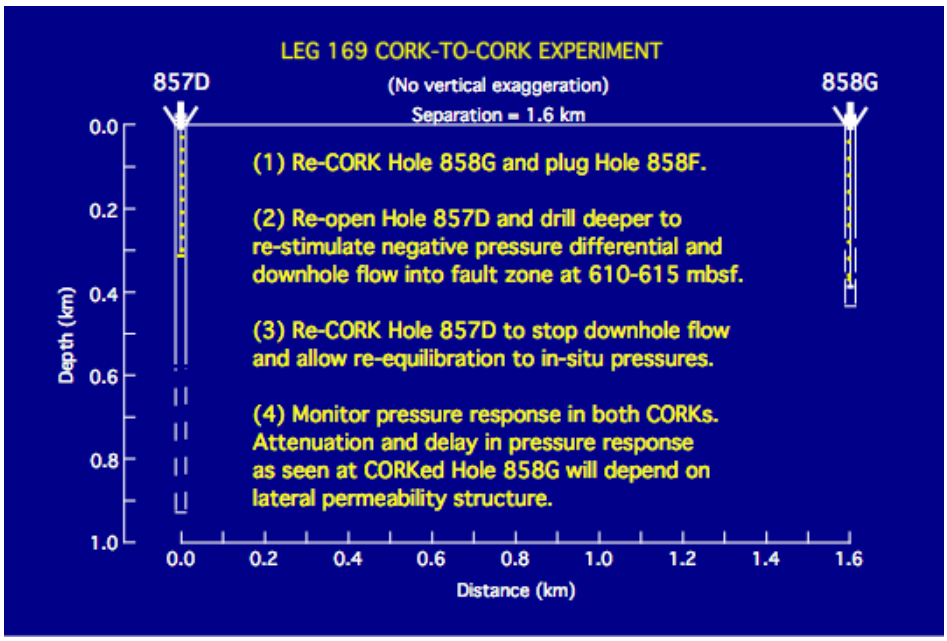

Figure 7.1. Explanation of the Hole 857D to 858G planned experiment. (Becker, pers. comm.)

Concurrent with drilling operations during Leg 169, an Ocean Bottom Seismometer (OBS) array was deployed in Middle Valley around Sites 857 and 858, with the purpose of determining the effects of drilling, if any, on microseismicity in mid-ocean ridge systems (Golden et al., 2003).

7.2 Holes 857D and 858G

While both sites are located in southern Middle Valley and are only separated by ~1.6 km, the difference in hydrologic regimes between these two sites is rather remarkable. Hole 857D is the deeper 'background' hydrothermal site, exhibiting a ~300kPa formation underpressure relative to seafloor hydrostatic, has a hydrologic basement defined by interbedded sediments and basaltic sills, and contains several zones of extremely high permeability that are inferred to be fault zones deep in the hole (Langseth and Becker, 1994). 858G on the other hand is a hydrothermal upflow site, with a slightly thinner sediment cover, as it is situated over a basement edifice. Hole 858G exhibits a ~180kPa overpressure relative to seafloor hydrostatic (Figure 7.2) (Davis and Becker, 1998) and has a hydrologic basement consisting of continuous basaltic flows. In this way it is more analogous to crust at unsedimented ridges (Becker, Morin, and Davis, 1994). Basement is highly fractured with a bulk permeability of 1-4 x 10^{-14} m^2, similar to that observed at the bottom of Hole 857D, and there are several highly transmissive zones with permeabilities estimated an order of magnitude greater than bulk permeability (Becker, Morin, and Davis, 1994).

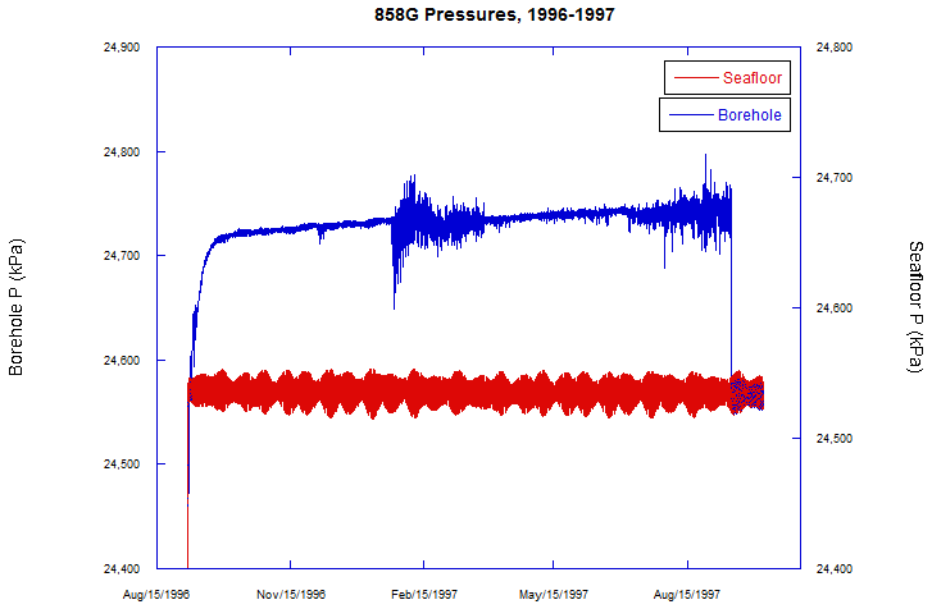

Figure 7.2. Raw pressure record from Hole 858G, 1996-1997. Note the sharp drop in borehole pressure in late September, 1997 that indicates unsealing of the hole.

7.3 Operational Timing During Leg 169

Leg 169 began on August 22, 1996 and its first goals were to remove the damaged CORK body at Hole 857D and replace the CORK body at Hole 858G. The Hole 858G CORK was replaced following a period of rough weather, during which coring took place at Hole 856H (Bent Hill Massive Sulfide site), and the new CORK body was latched in at 10:45 GMT on Sept. 5. Borehole fluid temperature observed with the Water Sampling Temperature Probe (WSTP) at 7 mbsf was above its limit of 150ºC. Another temperature tool (the Becker tool) was then deployed to 205-220 mbsf where a constant 273ºC fluid temperature was recorded (Shipboard Scientific Party, 1998a), indicating that the hole was producing prior to re-instrumentation. The ship then moved to Hole 857D and stabbed over the CORK body at 04:45 on Sept. 6. The damaged CORK body was removed, leaving the 300m thermistor cable in the open hole and necessitating fishing in the hole to retrieve it (>200m were recovered). Initial removal operations of the old CORK were completed as of 23:45

on Sept. 7, followed by a period of two days where the hole was left open, as the expedition moved back to drill at the Bent Hill Massive Sulfide deposit (Hole 1035A), one of the other main objectives of the expedition.

Replacement of the Hole 857D CORK body resumed at 05:00 on Sept. 10, 1996. After the hole was reentered, silt stirred up in the water was observed going into the hole, indicating the hole was still taking water. A sinker bar was run into the open hole to 642 mbsf and a temperature tab showed the temperature to be less than its threshold of 108ºC (Shipboard Scientific Party, 1998a). In the course of checking hole depth and still searching for pieces of the old thermistor cable, several regions of the hole were impassable with the drillstring, which necessitated washing and reaming the hole within casing between 359 and 446 mbsf (12:45 – 14:15 GMT) and outside casing between 611 and 929 mbsf (17:45 – 22:15 GMT) on Sept. 10. This process used seawater pumped down the drillstring by surface pumps to help circulate and clear any obstructions in the hole, here at a maximum pumping rate of ~90 strokes per minute (SPM). Following washing/reaming in the hole, the WSTP was lowered on the coring line to take a borehole fluid sample at 621 mbsf. The recovered sample was chemically identified as seawater with a temperature of 2ºC (Shipboard Scientific Party, 1998a). Downhole flow had clearly been stimulated by both leaving the hole open for several days and by injecting cold seawater into the borehole's deeper regions during washing. Initially the hole was to be deepened to help stimulate flow into the highly permeable zones observed during Leg 139; however poor weather conditions, the presence of observed strong downhole flow, and the other pressing goals of the expedition prevented any further drilling at Hole 857D. Re-CORKing resumed and the new CORK body was latched in at 14:00 GMT on Sept. 11, 1996.

7.4 Data: Pressures from Hole 858G after Replacement

The formation pressure data record from Hole 858G immediately following its installation essentially follows the same trend that we have observed at all other CORKs after installation: drilling-induced pressure perturbations linger, but formation pressure gradually returns to its pre-drilling state. In the case of Hole 858G (Figure 7.3) this means a gradual rise in formation pressure, as the ~180kPa overpressured formation recovers from the effects of perturbations by dense, cold seawater. However, between 06:00 and 07:00 GMT on Sept. 7, a negative pressure transient occurred (~36 kPa), and over the course of the following four days (Figure 7.4), formation pressure underwent several other rapid changes (Table 7.1) of varying magnitudes, both positive and negative. It is important to note that the overall trend of formation pressure is still the same (recovery from drilling conditions) and that these transients are superimposed on that trend. After Sept. 10, no further significant pressure transients were recorded for the remainder of 1996. Were drilling operations and the open hole at Hole 857D the cause of these pressure transients, or were there additional geologic phenomena that contributed to the observed transients?

7.5 Data: Microseismicity Recorded by OBS Array

Analyses and interpretation of the seismic events recorded by the OBS array located in Middle Valley during Leg 169 comprised the entirety of a doctoral dissertation by C. Golden (2000). The data presented in this section were once thought lost (as Dr. Golden has left academia and is unreachable by myself and his former collaborators) but were eventually found archived at the Scripps Institution of Oceanography, albeit incomplete. However, the most important data were recovered: the timing of seismic swarms that

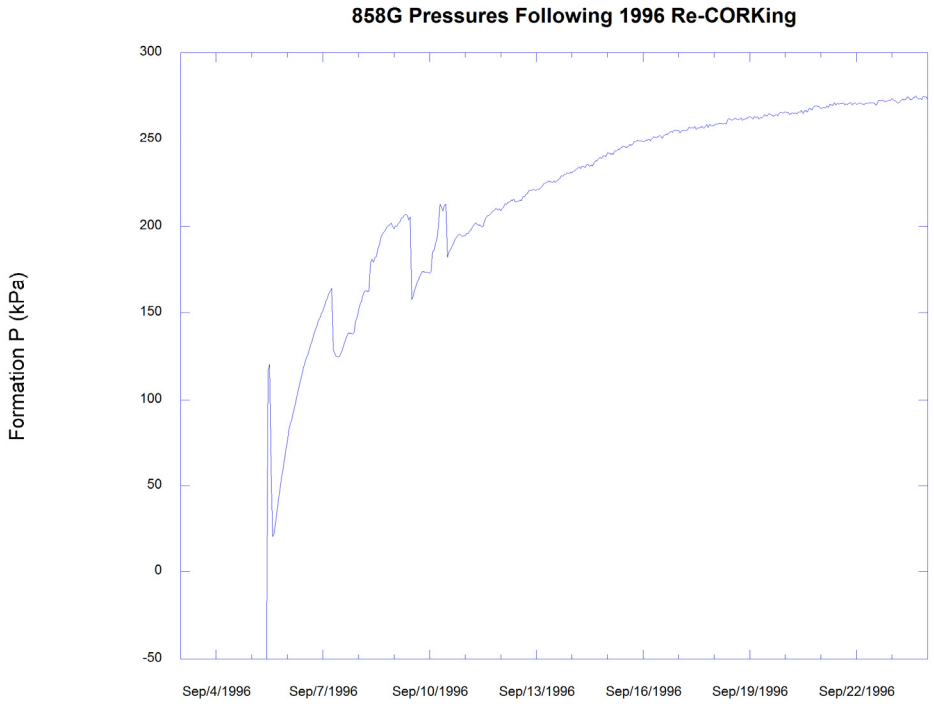

Figure 7.3. Relative formation pressure record from Hole 858G over the entirety of Leg 169. Note that this record has had seafloor loading removed.

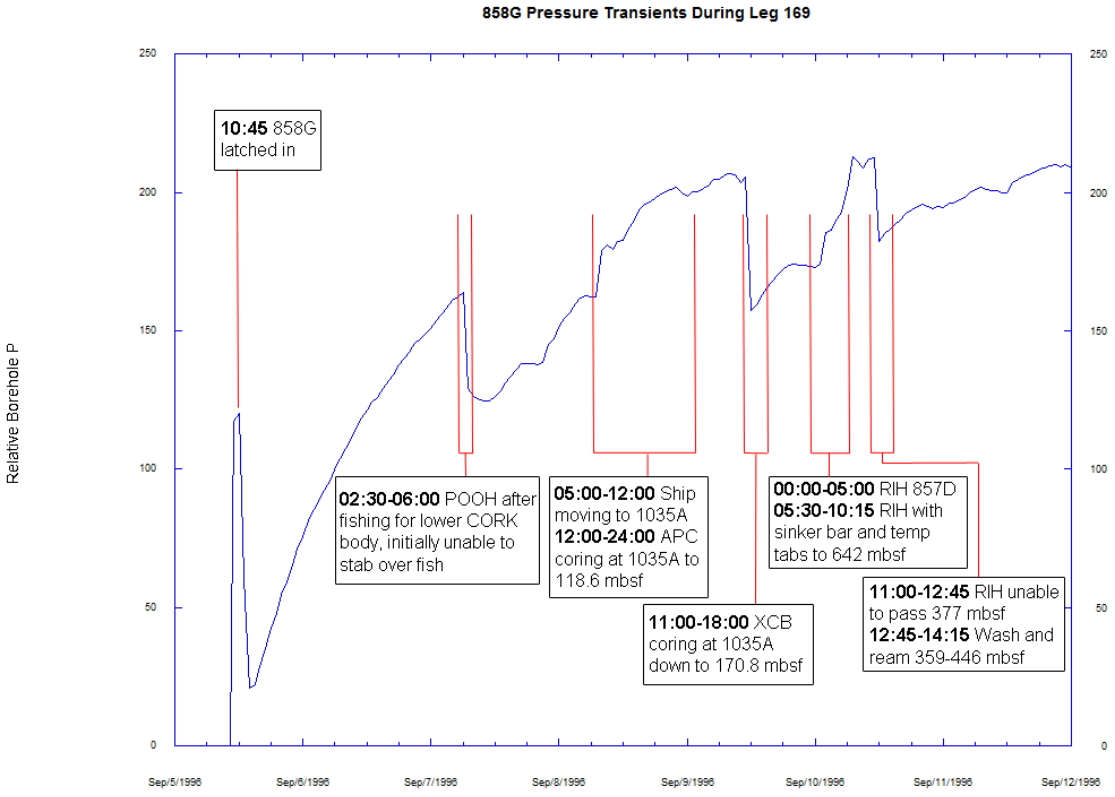

Figure 7.4. Relative formation pressure record with Leg 169 drilling operations overlaying the observed transients.

Formation Pressure Transients at 858G during Leg 169

Date/Time	Change in 858G Formation P	Leg 169 Operations
9/7/1996 06:00 - 07:00	~36 kPa decrease	Upper 857D CORK body already removed, drill string pulling out of hole after initial fishing for the lower CORK body
9/8/1996 07:00 - 08:00	~16 kPa increase	Drill string not in hole, ship moving to Hole 1035A (Bent Hill)
9/9/1996 11:00 - 12:00	~48 kPa decrease	XCB coring below 118.6 mbsf in Hole 1035A (Bent Hill)
9/10/1996 01:00 - 02:00	~11 kPa increase	Drill string run in below rig floor, but had not reentered 857D
9/10/1996 06:00 - 07:00	~11 kPa increase	Drill string run in 857D with sinker bar and temperature tabs
9/10/1996 11:00 - 12:00	~30 kPa decrease	Drill string run in 857D, obstruction at 377 mbsf

Table 7.1. Pressure transients at Hole 858G during Leg 169 and drilling operations that were occurring at the time.

occurred during Leg 169, previously only identifiable as a histogram in Golden, Webb, and Sohn (2003) (Figure 7.5). Migrated hypocenter data are unavailable for the events recorded; unmigrated data were recovered, but re-computing these data is outside the scope of this work.

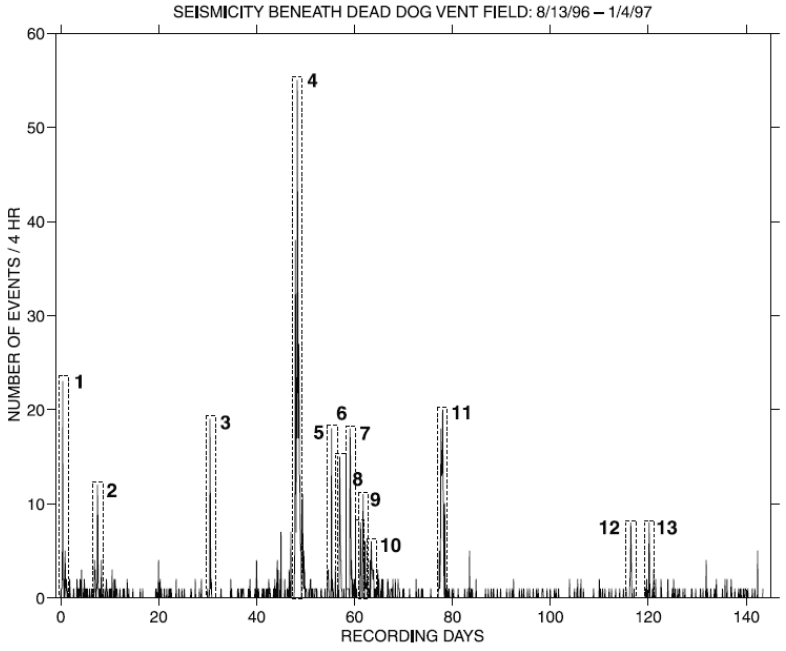

Figure 7.5. Histogram of 1996 microseismicity recorded in Middle Valley by the OBS array. From Golden, Webb, and Sohn, 2003. Recording Day 0 corresponds to August 12, 1996. Please refer to Table 2 for the date/time durations for each swarm.

Thirteen discrete microseismic swarms within Middle Valley were recorded by the OBS array (Table 7.2): nine of which were located around Sites 857 and 858 (Figure 7.6), and four of which (6, 7, 10, and 13) were located too far north of the array to have their hypocenters accurately calculated (Golden, 2000). In addition, there were other microearthquakes recorded by the array (shown as clear circles in Figure 7.6), however data regarding these events were not recovered. All of the calculated microearthquake hypocenters concentrate between 1 - 2.5 km depths in the crust (Golden, Webb, and Sohn, 2003) (Figure 7.7). How do these seismic swarms fit into the observations made at 858G? Were they the cause or the effect of transients observed, or were they completely unrelated?

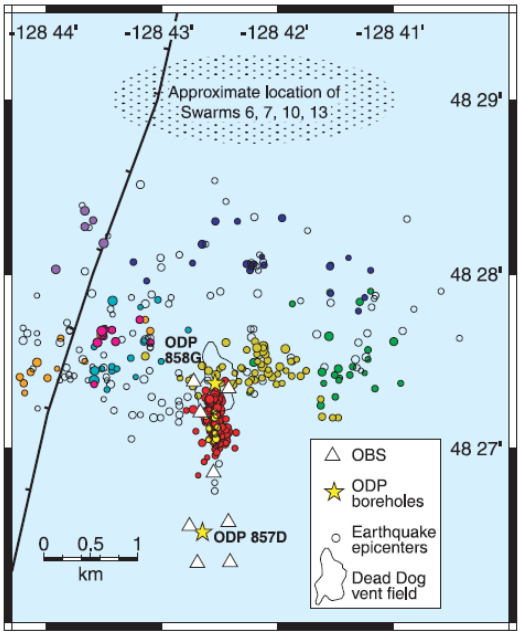

Figure 7.6. Map view of all microseismicity recorded by the 1996 OBS array. Clear circles indicate events not contained within one of the nine swarms. From Golden, Webb, and Sohn (2003).

Earthquakes Recorded by Middle Valley OBS Array

Swarm	Number of Events	Swarm Start (GMT)	Swarm End (GMT)
1	23	8/13/1996 19:40:24	8/15/1996 6:05:18
2	24	8/19/1996 21:16:56	8/21/1996 4:30:46
3	13	9/12/1996 22:29:32	9/13/1996 0:26:06
4	194	9/26/1996 14:48:34	10/2/1996 2:42:11
5	7	10/3/1996 9:23:22	10/4/1996 12:19:03
8	5	10/13/1996 15:42:16	10/13/1996 18:32:46
9	16	10/14/1996 5:35:21	10/15/1996 1:42:48
11	60	10/29/1996 14:27:08	10/30/1996 21:26:33
12	10	12/7/1996 17:47:50	12/8/1996 0:14:30

Table 7.2. Microseismic swarm start and end times recorded during 1996, for all swarms around Sites 857 and 858. Swarms 6, 7, 10, and 13 were located too far north of the array to calculate accurate hypocenters.

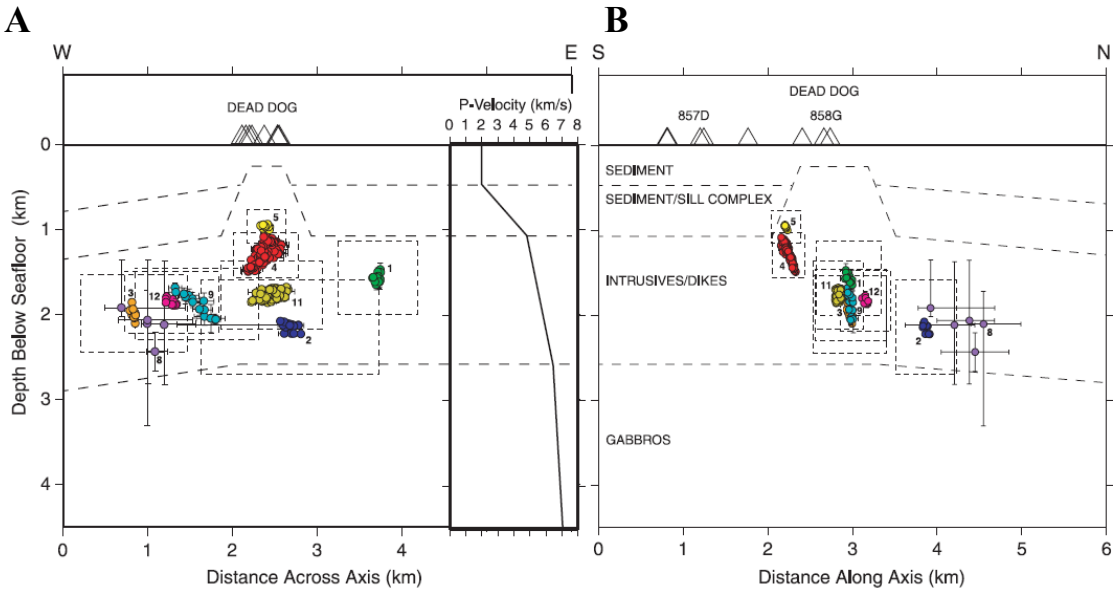

Figure 7.7. Migrated hypocentral data from the OBS array, both along a West-East transect (**A**) and a South - North transect (**B**). From Golden, Webb, and Sohn (2003).

7.6 Interpretation

1. Connections Between Microseismicity and Hole 858G Pressure Transients

If we consider the timing of the seismic swarms observed by the OBS array in Middle Valley (Table 7.2), it is immediately clear that they could not have caused the Hole 858G

pressure transients. As shown in Figure 7.8, all of the Hole 858G transients pre-date swarm #3 by several days, and occur several weeks after swarm #2. In fact, timing leads one to infer that processes that generated pressure transients at Hole 858G may also have played a role in microseismicity observed during Leg 169. It is interesting to note that microseismicity recorded by the OBS array is concentrated during Leg 169, and only one swarm (#11) with 20+ events was recorded after Leg 169 ended (and still had fewer than one-third the number of events as swarm #4). The swarms located closest to Hole 858G (#4, 5, 11) also appear to have little or no effect on borehole pressures. Since the Hole 858G transients and observed seismicity cannot be directly linked, one must consider drilling operations as an underlying cause to both.

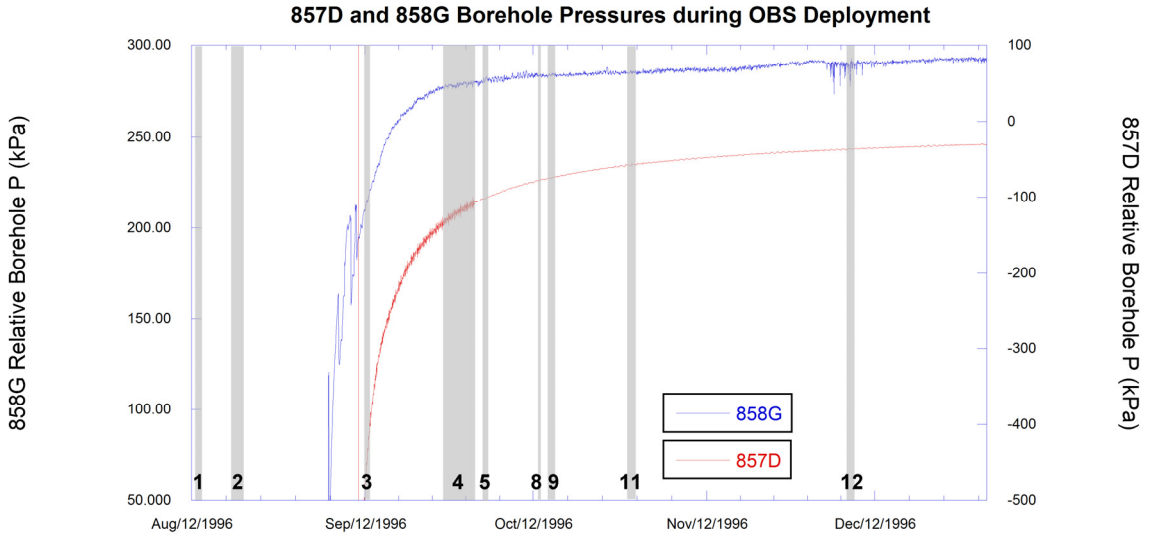

Figure 7.8. Microseismic swarms (shaded) recorded by the OBS array and their lack of influence on borehole pressure in both Holes 857D and 858G. Note that swarm 12, located somewhat close to Hole 858G, does appear to cause some pressure transients, however none of the swarms that occurred during Leg 139 or immediately afterwards elicit a significant pressure response in either hole.

2. Connections Between Drilling Operations and Hole 858G Pressure Transients

Considering the data presented in Table 1, it is clear that all the transients observed at Hole 858G occurred during the time when Hole 857D was unsealed, and the record immediately

returns to a normal recovery trend following latch-in of the new CORK body. In fact, the initial ~36 kPa transient observed coincides with Hole 857D becoming unsealed after pulling on the CORK body and removing the lower CORK from the hole. Later transients all occurred prior to Hole 857D being re-CORKed, and it is reasonable to assume that leaving the hole open and the resultant strong downhole flow observed contributed to perturbations in the local hydrothermal system, which were expressed as both positive and negative pressure transients at Hole 858G. This cross-hole response also speaks to the connectivity of the basement between Holes 857D and 858G: at least between the highly transmissive zones observed deep in Hole 857D and shallow basement at Hole 858G, as they have similar bulk permeabilities. Cross-hole formation pressure transients have also been observed during drilling operations on IODP Exp. 301 on the eastern Juan de Fuca ridge flank. In that case, seawater injected into the crust during drilling at Sites 1301 and 1026 generated a pressure transient recorded by a CORK (Hole 1027C) 2.4 kilometers away, likely due to an upper basement sill that connects the sites (Fisher, Davis, and Becker, 2008).

To further consider the role of dense seawater drawn into the formation due to underpressure, recall that during Leg 139 the flow rate into the highly transmissive zone at 610 mbsf was calculated as $1x10^4$ L/min following packer tests (Shipboard Scientific Party, 1992a). If we assume that such a flow rate was sustained for the duration that Hole 857D was left open in 1996, then we can calculate the maximum volume of fluid that would have entered the formation due to downhole flow into the zone at 610 mbsf. Hole 857D was left open from 1645 (local) on Sept. 7 until 2200 (local) on Sept. 9, and the new CORK was not latched in until 0700 on Sept 11. Effectively, Hole 857D could have drawn water for the

duration, a maximum of 86.25 hours. Given the estimated flow rate determined during Leg 139, we can estimate a maximum volume of 5.18×10^7 L of cold seawater that could have potentially entered the formation at Hole 857D. The flow rate calculated in 1991 is dependent on the borehole being isothermal and cold (2ºC), which generates a differential pressure exceeding 1 MPa between the borehole and the formation (Shipboard Scientific Party, 1992a). However the likelihood of Hole 857D attaining these conditions immediately following unsealing is extremely low, thus the previously calculated volume should be considered an extreme upper endmember for fluid volume entering basement. It is more likely that such a pressure differential developed gradually until ideal conditions were reached for such rapid downhole flow.

In addition to the downhole flow induced and maintained by an underpressured borehole, seawater was also injected into Hole 857D during hole washing and reaming. Unlike a packer experiment, where all injected seawater is assumed to enter the formation (eg. Becker and Fisher, 2008), these periods of washing the hole can be regarded as upper limits for the amount of seawater potentially injected into the formation in addition to downhole flow, as some seawater may exit the hole in this case. To calculate any volume potentially injected during washing, we need to know the pumping rate (SPM) and the ship's pump displacement to convert to a volume per time value. The JOIDES Resolution's mud pumps used for hole washing are triplex units, each of which has three pistons attached to a crank shaft. The displacement of the pump is equal to liner bore area × plunger stroke × number of pistons × crank shaft revolutions × pump efficiency. As currently configured, the mud pumps use three 16.5 cm diameter pistons and liners and have an efficiency of ~95%, therefore 1 SPM = 5.2 gallon/min or 0.33 L/s (Shipboard Scientific Party, 2010). As

previously described, washing at two depth intervals occurred on Sept. 10, and average pumping rates were determined from the engineering logs for that day. The upper interval (359-446 mbsf) was washed for ~90 minutes at a rate of ~85 SPM (~1683 L/min). The lower interval (611-929 mbsf) was washed for ~270 minutes at a rate of ~90 SPM (~1782 L/min). Thus the maximum volume of seawater that could have entered the formation due to washing at both depth intervals was 6.3×10^5 L. It is important to note here that this calculated volume is two orders of magnitude smaller than the fluid volume drawn downhole due to underpressure, but over a much shorter timescale (hours as opposed to days). However, some or most of this washing-injected seawater may have exited the hole instead of going into the formation, especially during washing the shallow interval. Based on the record from Hole 858G, the final transient does appear to coincide with washing of the shallow interval in Hole 857D, however no pressure transient resulted from washing the deep interval, which would be expected considering its high permeability and apparent connectivity with basement at Hole 858G. Potentially, washing the upper interval within casing cleared whatever constriction was preventing more rapid downhole flow into the highly transmissive region in the open hole and caused the final Hole 858G anomaly. We must thus consider that: (1) flow due to formation underpressure, rather than fluid injection directly related to drilling operations at Hole 857D, was the major source of the pressure transients at 858G, or (2) downhole flow into Hole 857D was restricted due to a blockage in the casing, and when removed by washing reopened the enhanced connectivity between the two holes.

Looking at the pattern of pressure transients recorded at Hole 858G and Leg 169 operations, we can only tie one drilling event unequivocally to the transients observed

(Figure 7.9). The first -36 kPa transient occurred during fishing for the lower Hole 857D CORK body after the removal of the damaged upper CORK body, and was likely the result of the unsealing of that hole, causing a rapid dilatation of the pressurized formation. Indeed this transient looks remarkably like the dilatational response observed at Hole 857D in 2001 to local seismicity (Figure 7.9) which clearly showed a coseismic elastic dilatation followed by hydrologic diffusion (Davis et al., 2004). By treating the pressure change due to unsealing 857D as a result of internal plate deformation, which is aseismic in this case, we can calculate the volumetric strain generated at this time as described in Chapter 6 (Davis et al., 2001). Strain generated by unsealing Hole 857D is calculated to be -1.05 x 10^{-5}, based on the previously mentioned constants and equations. The strain-induced pressure gradient generated between the two sites helped drive fluid into the formation at Hole 857D, initiating the pressure recovery at Hole 858G that followed. This response to the initial dilatational strain coupled with the initiation and stimulation of downhole flow into the open Hole 857D, may have helped to produce a positive pressure response at Hole 858G superimposed on the already steadily recovering formation pressure. However this conjecture is purely speculative, as are those that follow.

I. Other Hydrologic Events Following Unsealing

After the unsealing of Hole 857D, the pressure record from Hole 858G tells a story that is less clear. The -48 kPa transient on Sept. 9 occurred during XCB coring in Hole 1035A at the Bent Hill Massive Sulfide deposit, which is located farther from Hole 858G than Hole 857D. Basement was not penetrated in this hole, nor was the silicified layer thought to be a

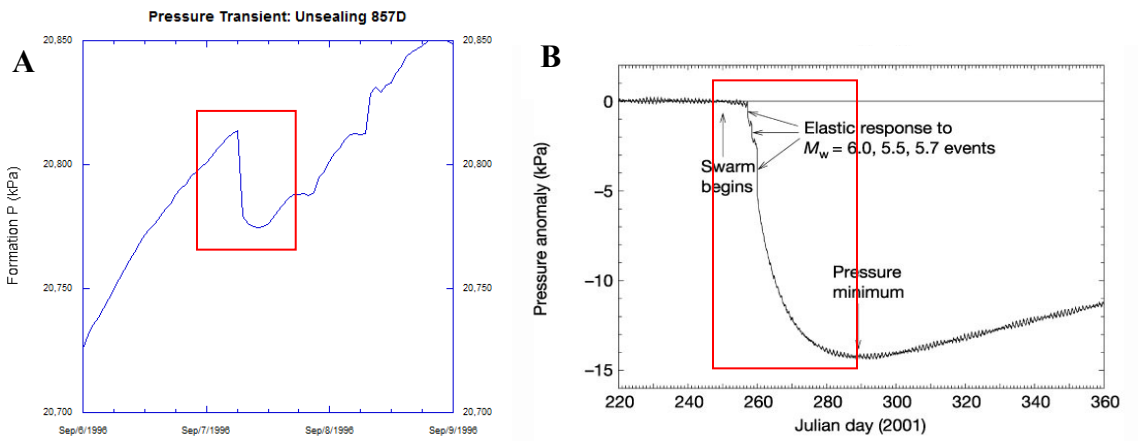

Figure 7.9 A. Pressure record from Hole 858G showing only the transient associated with unsealing Hole 857D in 1996. Diffusive response is superimposed on the recovering pressure trend in the borehole. **B.** Hole 857D's elastic and subsequent diffusive response to coseismic strain in Middle Valley in 2001 (from Davis et al., 2004). Seafloor loading has been removed from both datasets and the red boxes enclose the areas of interest/similarity.

barrier between primary and secondary fluid circulation cells in the rift valley (Wheat and Fisher, 2007). This silicified layer was penetrated in several other holes at a later date in Leg 169, with no apparent effect on Hole 858G pressures, removing drilling operations as a link to this transient. However it is of a similar magnitude as transients observed during the first year of pressure observations at Hole 858G in 1991-2, which occurred after CORK installation in Middle Valley on Leg 139. Two of these earlier transients were coupled with a cooling trend in some part of the borehole (Davis and Becker, 1994), and at the time were attributed to the nearby Hole 858F (later plugged) which had become a synthetic vent that was thought to have short circuited local hydrothermal circulation and drawn down some volume of seawater into the nearby formation. However it may also be possible that these "hydrologic events," as they are referred to by Davis and Becker (1994), are the result of a strong hydrologic connection between basement at Holes 857D and 858G that we have not quantified; the strongly underpressured Hole 857D serving as a source to pull cold

seawater into the formation when open, and allowing perturbations farther afield to occur and persist if the hole is left open long enough.

For the unexplained ~48 kPa and ~36 kPa transients that occurred during Leg 169, these may be purely a consequence of downhole flow due to underpressure. Owing to the already established permeability similarities of basement between Holes 857D and 858G and the absence of reasonable drilling operations to explain the transients, these instantaneous events can only be related to the influx of a large volume of cold (2ºC) seawater (due to downhole flow into Hole 857D and possibly Hole 1035A) into an isothermal (270ºC) hydrothermal reservoir, which may have started localized cracking fronts in the formation thereby creating new volume, causing localized dilatation. This kind of cracking phenomenon has been observed in terrestrial boreholes where hydrofracturing of hot reservoir rock due to cold fluid injection is one of the main processes used in geothermal energy production, often generating localized microseismicity in the process (eg. Zoback and Harjes, 1997; Shapiro and Dinske, 2009). Basement at Site 858 was observed as highly fractured during Leg 139, so hydrofracturing due to thermal shock in the formation is not an inconceivable notion to consider here, but can thermal contraction alone produce a pressure decrease? Cold fluid injected into the borehole would produce an initial positive pressure anomaly, and in a confined system would cool basement enough to cause fracturing: especially in an extensional environment such as Middle Valley, where basement is already close to failure. However the subsequent warming of the injected fluid would produce a pressure increase that might offset some or all of the pressure decrease resulting from dilatation by hydrofracture. If these two competing effects balance out, this could leave the cold-hole input (in this case at

Hole 857D) as the dominant signal observed and produce a “cold finger” effect extending into basement. Davis and Becker (1994) allude to seawater influx as a source for localized fracturing, but cite Hole 858F as the most likely intake since it is located nearest to Hole 858G. However when Hole 858F was plugged, no visible change in pressure or temperature was recorded by Hole 858G. At the time this was believed to be due to the inadequacy of the plug, however if the seawater intake had been from the initial drilling of Hole 857D, then the persistent thermal anomaly observed in the shallow Hole 858G borehole temperature record (Davis and Becker, 1994) could be due to that water mass, as opposed to water from Hole 858F. In 1996, the initial unsealing of Hole 857D and subsequent days when it was open to bottom seawater may have resulted in the intake of a large mass of water (potential volumes mentioned previously) that persisted in the hot crust and occasionally caused local fracturing events. Note that all large pressure transients (and by association, events) cease once Hole 857D is once again sealed. This indicates that underpressure and the hydrologic connection between Holes 857D and 858G, while not completely understood or quantified, is the more likely cause for the second and third dilatational pressure transients observed rather than a direct connection to drilling operations.

3. Connections Between Microseismicity and Drilling Operations

Golden (2000) attributed the bulk of the observed swarms to a hydrothermal cracking front below Dead Dog vent field (Site 858), as the earthquakes observed were quite deep (>1.0 km below seafloor) and for the most part were located around Site 858 rather than 857. He hypothesized that the cracking front was the result of seawater recharge along one of the many normal faults in Middle Valley, here specifically the central fault (Golden, Webb,

and Sohn, 2003). However, the timing of the microseismicity, drilling operations, and borehole pressure transients due to an open, underpressured borehole are far too coincidental to be completely unrelated, as Golden implies in his analysis. We have already estimated the volume of seawater drawn into Hole 857D through downhole flow and strain-induced flow into the underpressured borehole, and also the added injection of seawater during the process of washing and reaming the hole prior to re-CORKing. Additionally, we know that basement in Middle Valley is hot (~270ºC), and at Site 858 is heavily fractured, and composed of continuous basaltic flows, resembling basement at an unsedimented ridge, so hydrofracturing due to seawater recharge is a distinct possibility. However, Golden never considers the role of drilling and/or an open, underpressured borehole intersecting a highly transmissive fault zone in his assessment of microseismicity.

Seawater recharge along rift-valley bounding normal faults in Middle Valley is known to occur (Wheat and Fisher, 2007), and is probably an important source of recharge for fluid circulation in the valley (Stein and Fisher, 2001). However, the rate of recharge is unknown for most faults in Middle Valley. Modeling based on porefluid geochemistry from Site 855 (eastern boundary fault) gives a recharge rate of ~9 m^3/yr per meter of fault that is recharging, but concluded that even if 17 km of the fault was recharging at this rate, that volume could only account for 3% of the total volume needed to sustain the vent fields present in Middle Valley (Wheat and Fisher, 2007). Comparing this calculated boundary fault recharge rate to the flow rate into Hole 857D at 610 mbsf ($1x10^4$ L/min, or 10 m^3/min), it is clear that flow into Hole 857D is far more rapid than observed recharge at local normal faults and must be playing a more significant role in any hydrofracturing that is occurring. In addition, looking at the location pattern of earthquake swarms observed

(Figure 5), recharge from a bounding fault just does not fit with the timing and location of swarms: swarms 1 and 2 occur to the east of Site 858, then swarm 3 occurs ~1 km west of Site 858 (west of the central fault). One would expect that a hydrothermal cracking front influenced by recharge down a linear fault would not generate earthquake swarms quite so randomly. However, if we exclude swarms 1 or 2, as they occur prior to the start of Leg 169, and swarm 3, as it is located west of the central fault (Figure 7.10), the swarm pattern during September/October makes more sense.

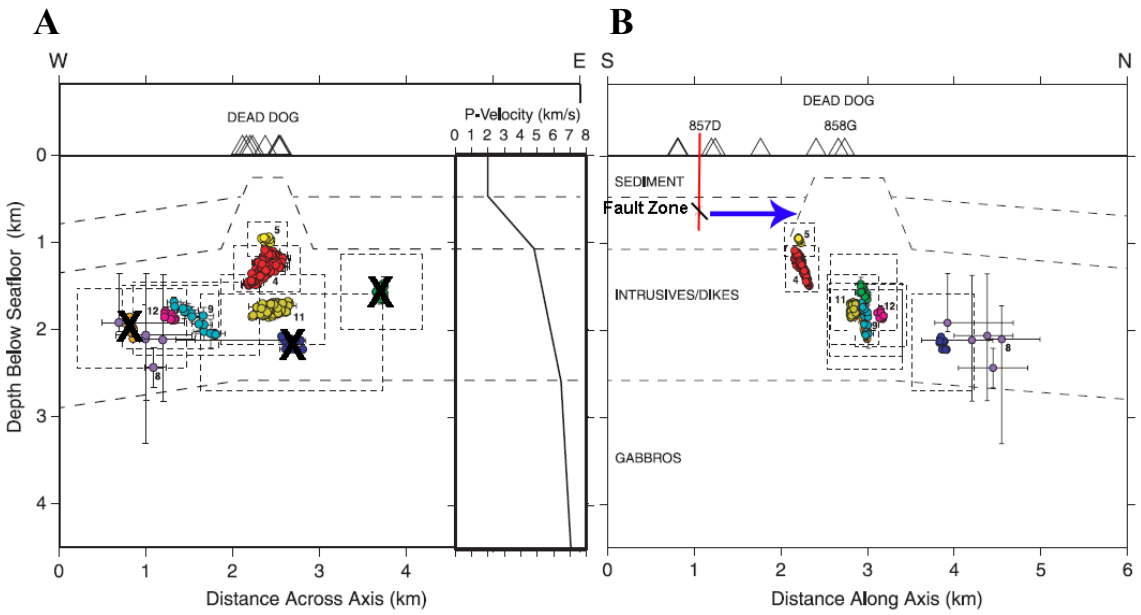

Figure 7.10 A. West to East transect of earthquake swarm locations with irrelevant swarms removed (see text for further discussion). **B.** Along-strike (South to North) transect of swarm locations. Red line indicates the borehole at Hole 857D crosscutting a fault zone at 610 mbsf, and the blue arrow indicates implied direction of flow based on fluid pressure responses at Hole 858G while Hole 857D was open to bottom seawater influence. Modified from Golden, Webb, and Sohn, 2003.

As previously established, following the unsealing of Hole 857D, inflow of cold, dense seawater into the formation began. Superimposed onto Hole 858G's recovery trend are instantaneous pressure decreases assumed to be related to some amount of localized hydrofracturing that may or may not be offset by a pressure increase from warming the injected fluid. We know that a large volume of water was injected over a period of days,

but we do not know its long-term fate once in the formation. While we know that Hole 857D is well connected to shallow basement at Site 858, Hole 858G extends less than 200 meters into basement. Thus it is difficult to say what the permeability structure of the deeper basement is like. However, if we assume that the microseismicity under Site 858 was all due to hydrofracturing, as Golden suggests, then we can follow the water in the crust as it interacted with hot rock, which cooled, contracted, and created more fracture space for fluid to flow. This fracture propagation should create a pattern of microseismicity based on flowpath (Shapiro and Dinske, 2009). Swarm 4, comprising 194 separate events, began ~2 weeks after 857D was sealed. However, within swarm 4 are smaller groupings of events that indicate microseismicity did not happen all at once: 7 closely set events on Sept. 26, then 10 hours later 6 more closely set events on Sept. 27, then 2 days passed before 5 more closely set events on early Sept. 29, then 113 events on Sept. 30, 63 more events on Oct. 1, and finally concluding the swarm with 3 events on Oct. 2. This alludes to stepwise propagation of hydrofracturing in basement, but without knowing the hypocentral depths for each event, it is hard to say how this propagation occurred (deep to shallow or otherwise). It is important to note here that no pressure transients were recorded by either Hole 857D or Hole 858G during this or most of the other microseismic swarms (the exception being swarm 12, see Figure 7.9), suggesting that any dilatation was too small or too isolated in the formation to have been felt by either borehole.

Looking at the geometry of swarm 4, its shape is roughly vertical; vertically oriented seismic swarms have previously been observed beneath several of the vent sites at 9ºN, and have been described as hydrothermal cracking fronts (Sohn, Hildebrand, and Webb, 1999).

At an unsedimented ridge, such an event would be due to recharge (which could be from anywhere since the ridge is bare rock), however here we have ruled out boundary-fault controlled recharge due to swarm locations and the small recharge volumes estimated, making the only possible source for fluid-induced seismicity the pulse of seawater from Hole 857D. Further evidence for fluid propagation is swarm 5, which occurred on Oct 4-5 and was located immediately above swarm 4. It is unclear if any of the later swarms are related to the seawater influx at Hole 857D, as they occur much later and are generally deeper than swarms 4 and 5. However given the timing and location of microseismicity observed during and immediately after Leg 169, (Figure 7.9) it is clear that at least some of the swarms were caused by the flux of cold seawater into basement not via fault-controlled recharge as postulated by Golden, but by drilling and underpressure-induced flow into Hole 857D.

7.7 Discussion/Summary

The Leg 169 cross-hole experiment in Middle Valley, while simple in scope, yielded a complex result unlike other cross-hole crustal-scale experiments. After leaving Hole 857D open to stimulate downhole flow, several large pressure decreases and subsequent recoveries were observed at Hole 858G, much like the "hydrologic events" mentioned by Davis and Becker (1994) but there was not a persistent long-term trend due to a pulse of cold seawater from Hole 857D; hole recovery from drilling perturbations resumed as expected once Hole 857D had been re-CORKed. This tells us that there is connectivity between basement at these 2 sites that we do not completely understand. While the effects of (1) the rapid dilatation during the unsealing of Hole 857D and (2) potential

local hydrofracturing while Hole 857D remained open were recorded by Hole 858G, no pressure changes were observed by either CORK during all but one of the hydrofracturing events co-located with microseismicity. This says that we currently do not have a complete understanding of permeability anisotropy in the Middle Valley hydrothermal system. In addition, the presence of the OBS array in Middle Valley during drilling provides a look into the effect that drilling has on the hydrothermal system outside of the pressure/temperature changes we can observe with a CORK, although the incompleteness of the 1996 OBS data makes it difficult to pin specific drilling operations to observed seismicity. There were a large number of hypocenters that did not fit into a swarm, and it would be interesting to see, if those data still exist, if any of those microearthquakes were related more directly to operational events.

Currently, the CORK at Hole 858G is not recording pressure data. After the data logger stopped responding to communications in 1999, it was observed on subsequent dives covered in flocculent microbial mats, indicating that the CORK seals had failed and flow up the borehole was occurring. With the technological improvements in CORK engineering in the last decade, it would be very useful to re-instrument Hole 858G (perhaps deepening the hole in the process) and possibly conduct another cross-hole experiment, this time with a few more controls on the variables (use a packer, controlled injection rate, time, etc). Doing controlled packer slug and/or injection tests would help our understanding of the connection between Sites 858 and 857, the vertical permeability structure within basement, and how hydrothermal circulation in Middle Valley actually occurs (ie. does it fit the published model?). Additionally Hole 858G, located in an upflow zone, would be an ideal location to deploy subseafloor geochemical samplers and

microbial colonization experiments in order to investigate subseafloor processes. As mentioned in previous chapters, Hole 857D is still recording data, and its ~4.5 year period of uplift could be heralding an impending eruption event. Re-instrumenting Hole 858G even on a rudimentary level would be ideal for collecting any data from such an event, in the hopes of learning as much as possible about the eruptive cycle of sedimented ridges.

ADDENDUM AND FUTURE WORK

Post-defense analyses of Hole 857D high-resolution logger data downloaded in September 2012 indicate that the downhole logger's seafloor record may in fact be an artifact of gauge failure or drift, as opposed to an actual uplift signal, despite the corroborating Alvin depth data. This type of artifact has not been observed previously and we do not yet know the cause. Also, the apparent depth decrease recorded by the Alvin pressure gauge is especially perplexing, but we know nothing about the Paroscientific sensor installed on the submersible or the characteristics of its drift over time so it is unclear whether or not this decrease is real. On the other hand the borehole data have been verified, as the trends between both loggers' records match for the time period of data overlap (2010-2012). As mentioned in Chapter 6, if the uplift signal is not real then we must consider alternative theories for what caused the dramatic change in hydrothermal venting in Middle Valley between 2008 and 2010, as well as the 2005-2012 drop in formation pressure.

This dissertation in no way completes our understanding of the hydrogeology of Middle Valley as a sedimented rift. In fact it raises more questions than it answers, necessitating further long-term research and monitoring. Some of this monitoring is already in progress: both pressure data loggers at Hole 857D are active and recording data, OBS and OBH units have recently been deployed in the region, and the NEPTUNE Canada cabled observatory is pursuing funding to instrument a node in Middle Valley. However, if we are to answer the fundamental questions brought up by the research contained in this dissertation, there is still a great deal of work to be done.

In light of the newest data recovered from the Hole 857D high-resolution logger, it is clear that a fine scale (<1 m) bathymetric map of the southern part of Middle Valley is needed to allow us to track any potential future deformation. Coupled with this map would be the installation of several more "benchmarks" like those on Axial Volcano. One of these benchmarks could be a re-instrumented Hole 858G, also giving us more long-term data about the hydrogeology of the system overall. On a larger scale, determining the role of West Valley magmatism, if any, in Middle Valley is of obvious interest, given the similar basalt petrologies. Seismic surveys of the crustal structure beneath both West and Middle Valleys might yield new clues to their magmatic connectivity, if any exists.

Experimentally, readdressing the connectivity between Holes 857D and 858G would be a worthwhile pursuit. Designing an injection test (perhaps similar to the one performed during IODP Expedition 327) with carefully timed injections and rates, and possibly injected tracer chemicals would put us well on the path to constraining some of the more speculative interpretations of basement connectivity in Chapter 7 of this dissertation.

Additionally, this dissertation has mainly addressed the geophysical aspects of the Middle Valley system. It would be beneficial to incorporate any geochemical data from the region in order to address the accuracy of the current hydrothermal circulation model. These data could also aid in potentially understanding the eruptive cycle for the region. Did vent fluid chemistry at Dead Dog field change at all between 2005 and 2010? And if so, does this reflect a change in reaction zone depth, phase separation, or other variables that have been observed to change systematically during an eruptive cycle?

Finally, readdressing the role of drilling in inducing local microseismicity seems to be warranted, judging by the tenuous connections made in Chapter 7. Revisiting the original 1996 OBS data and including all the recorded microseismicity would go a long way to addressing this. Did any of the events match up with drilling operations? Golden did not consider the connection between the two significant; but I feel strongly that this should be reconsidered.

REFERENCES

Alt, J. C. (1995), Subseafloor processes in mid-ocean ridge hydrothermal systems, *in Geophysical Monograph Series vol. 91: Seafloor Hydrothermal Systems: Physical, Chemical, Biological, and Geological Interactions*, vol. 91, edited by S. E. Humphris, R. A. Zierenberg, L. S. Mullineaux, and R. E. Thomson, pp. 85–114, American Geophysical Union, Washington, D. C.

Ames, D. E., J. M. Franklin, and M. D. Hannington (1993), Mineralogy and geochemistry of active and inactive chimneys and massive sulfide, Middle Valley, Northern Juan de Fuca Ridge - an evolving hydrothermal system, *Canadian Mineralogist*, *31*, 997–1024.

Annen, C. (2011), Implications of incremental emplacement of magma bodies for magma differentiation, thermal aureole dimensions and plutonism–volcanism relationships, *Tectonophysics*, *500*(1-4), 3–10, doi:10.1016/j.tecto.2009.04.010.

Becker, K., R. H. Morin, and E. E. Davis (1994), Permeabilities in the Middle Valley hydrothermal system measured with packer and flowmeter experiments, *Proc. Ocean Drill. Program Scientific Results*, College Station, TX (Ocean Drilling Program), *139,* 613-636.

Butterfield, D., R. McDuff, J. Franklin, and C. G. Wheat (1994), Geochemistry of hydrothermal vent fluids from Middle Valley, Juan de Fuca Ridge, *Proc. Ocean Drill. Program Scientific Results*, *139*, College Station, TX (Ocean Drilling Program), 395–410, doi:doi:10.2973/odp.proc.sr.139.266.1994.

Canales, J. P., H. Carton, S. M. Carbotte, J. C. Mutter, M. R. Nedimović, M. Xu, O. Aghaei, M. Marjanović, and K. Newman (2012), Network of off-axis melt bodies at the East Pacific Rise, *Nature Geoscience*, *5*(4), 279–283.

Carbotte, S. M., M. R. Nedimović, J. P. Canales, G. M. Kent, A. J. Harding, and M. Marjanović (2008), Variable crustal structure along the Juan de Fuca Ridge: Influence of on-axis hot spots and absolute plate motions, *Geochemistry Geophysics Geosystems*, *9*(8), doi:10.1029/2007GC001922.

Chadwick, W. W., D. J. Geist, S. Jónsson, M. Poland, D. J. Johnson, and C. M. Meertens (2006a), A volcano bursting at the seams: Inflation, faulting, and eruption at Sierra Negra volcano, Galápagos, *Geology*, *34*(12), 1025.

Chadwick, W. W., S. L. Nooner, M. A. Zumberge, R. W. Embley, and C. G. Fox (2006b), Vertical deformation monitoring at Axial Seamount since its 1998 eruption using deep-sea pressure sensors, *Journal of Volcanology and Geothermal Research*, *150*(1-3), 313–327.

Curray, J., and D. G. Moore (1982), *Initial Rep. of the DSDP*, *64*, doi:doi: 10.2973/dsdp.proc.64.1982.

Davis, E., and K. Becker (1999), Tidal pumping of fluids within and from the oceanic crust: new observations and opportunities for sampling the crustal hydrosphere, *Earth and Planetary Science Letters*, *172*(1-2), 141–149.

Davis, E., K. Becker, R. Dziak, J. Cassidy, K. Wang, and M. Lilley (2004), Hydrological response to a seafloor spreading episode on the Juan de Fuca Ridge, *Nature*, *430*(6997), 335–338.

Davis, E. E., and K. Becker (1994), Formation temperatures and pressures in a sedimented rift hydrothermal system: 10 months of CORK observations, Holes 857D and 858G, *Proc. Ocean Drill. Program Scientific Results*, *139*, 649–666.

Davis, E. E., D. S. Chapman, C. B. Forster, and H. Villinger (1989), Heat-Flow Variations Correlated with Buried Basement Topography on the Juan-De-Fuca Ridge Flank, *Nature*, *342*(6249), 533–537.

Davis, E. E., and A. T. Fisher (1994), On the nature and consequences of hydrothermal circulation in the Middle Valley sedimented rift: inferences from geophysical and geochemical observations, Leg 139, *Proc. Ocean Drill. Program Scientific Results*, *139*, 695–717, doi:doi:10.2973/odp.proc.sr.139.259.1994.

Davis, E. E., W. D. Goodfellow, B. D. Bornhold, J. Adshead, B. Blaise, H. Villinger, and G. M. Lecheminant (1987), Massive Sulfides in a Sedimented Rift-Valley, Northern Juan-De-Fuca Ridge, *Earth and Planetary Science Letters*, *82*(1-2), 49–61.

Davis, E. E., and H. Villinger (1992), Tectonic and thermal structure of the Middle Valley sedimented rift, northern Juan de Fuca Ridge, *Proc. of the Ocean Drill. Program, Initial Reports*, *139,* 9-41.

Davis, E. E., K. Wang, R. E. Thomson, K. Becker, and J. F. Cassidy (2001), An episode of seafloor spreading and associated plate deformation inferred from crustal fluid pressure transients, *Journal of Geophysical Research-Solid Earth*, *106*(B10), 21953–21963.

Detrick, R. S., P. Buhl, E. Vera, J. Mutter, J. Orcutt, J. Madsen, and T. Brocher (1987), Multi-channel seismic imaging of a crustal magma chamber along the East Pacific Rise, *Nature*, *326*(6108), 35–41.

Dixon, T., M. Bursik, S. Wolf, M. Heflin, F. Webb, F. Farina, and S. Robaudo (1993), Constraints on deformation of the resurgent dome, Long Valley caldera, California from space geodesy, *Contributions of Space Geodesy to Geodynamics: Crustal Dynamics*, *Geodynamic*. *23,* 193-214.

Dziak, R. P., and C. G. Fox (1999), The January 1998 Earthquake swarm at Axial Volcano, Juan de Fuca Ridge: Hydroacoustic evidence of seafloor volcanic activity, *Geophysical Research Letters*, *26*(23), 3429.

Elderfield, H., C. G. Wheat, M. J. Mottl, C. Monnin, and B. Spiro (1999), Fluid and geochemical transport through oceanic crust: a transect across the eastern flank of the Juan de Fuca Ridge, *Earth and Planetary Science Letters*, *172*(1-2), 151–165.

Fisher, A., K. Fischer, D. Lavoie, M. Langseth, and J. Xu (1994), Geotechnical and hydrogeological properties of sediments from Middle Valley, northern Juan de Fuca Ridge, *Proc.of the Ocean Drill. Program, Scientific Results*, *139*, 627–647, doi:doi:10.2973/odp.proc.sr.139.246.1994.

Fisher, A. T. et al. (2005), Scientific and technical design and deployment of long-term subseafloor observatories for hydrogeologic and related experiments , IODP Expedition 301, Eastern flank of Juan de Fuca Ridge, *Proc. IODP, 301*, doi:10.2204/iodp.proc.301.103.2005.

Fisher, A. T. et al. (2011), Design , deployment , and status of borehole observatory systems used for single-hole and cross-hole experiments, IODP Expedition 327, Eastern flank of Juan de Fuca Ridge, *Proc. IODP*, *327*, doi:10.2204/iodp.proc.327.107.2011.

Fisher, A. T., E. E. Davis, and K. Becker (2008), Borehole-to-borehole hydrologic response across 2.4 km in the upper oceanic crust: Implications for crustal-scale properties, *Journal of Geophysical Research-Solid Earth*, *113*(B7), B07106.

Fornari, D., T. Shank, K. Von Damm, T. K. Gregg, M. Lilley, G. Levai, A. Bray, R. Haymon, M. Perfit, and R. Lutz (1998), Time-series temperature measurements at high-temperature hydrothermal vents, East Pacific Rise 9°49′–51′N: evidence for monitoring a crustal cracking event, *Earth and Planetary Science Letters*, *160*(3-4), 419–431.

Fouquet, Y., R. Zierenberg, D. J. Miller, and E. Al (1998), *Proc. Ocean Drill. Program, Init. Repts., 169*.

Fox, C. G., W. E. Radford, R. P. Dziak, T. Lau, H. Matsumoto, and A. E. Schreiner (1995), Acoustic detection of a seafloor spreading episode on the Juan de Fuca Ridge using military hydrophone arrays, *Geophysical Research Letters*, *22*(2), 131.

Golden, C. E. (2000), Investigation of Ocean Spreading Center Hydrothermal Processes Using Ocean Bottom Seismometers (Ph.D. dissertation, UC San Diego), 86 pp.

Golden, C. E., S. C. Webb, and R. A. Sohn (2003), Hydrothermal microearthquake swarms beneath active vents at Middle Valley, northern Juan de Fuca Ridge, *Journal of Geophysical Research-Solid Earth*, *108*(B1), 2027.

Hooft, E. E. E. et al. (2010), A seismic swarm and regional hydrothermal and hydrologic perturbations: The northern Endeavour segment, February 2005, *Geochemistry Geophysics Geosystems*, *11*(12), 1–23, doi:10.1029/2010GC003264.

Langseth, M. G., and K. Becker (1994), Structure of igneous basement at Sites 857 and 858 based on Leg 139 downhole logging, *Proc.of the Ocean Drill. Program, Scientific Results*, *139*, 573–583.

Mogi, K. (1958), Relations between the eruptions of various volcanoes and the deformations of the ground surfaces around them, *Bulletin of the Earthquake Research Institute*, *36*, 99–134.

Nooner, S. L., and W. W. Chadwick (2009), Volcanic inflation measured in the caldera of Axial Seamount: Implications for magma supply and future eruptions, *Geochemistry Geophysics Geosystems*, *10*(2), doi:10.1029/2008GC002315.

Okada, Y. (1985), Surface deformation due to shear and tensile faults in a half-space, *Bulletin of the Seismological Society of America*, *75*(4), 1135–1154

Pawlowicz, R., B. Beardsley, and S. Lentz (2002), Classical tidal harmonic analysis including error estimates in MATLAB using T-TIDE, *Computers & Geosciences*, *28*(8), 929–937, doi:10.1016/S0098-3004(02)00013-4.

Perfit, M., and W. W. Chadwick (1998), Magmatism at Mid-Ocean Ridges: Constraints from Volcanological and Geochemical Investigations, in *Geophysical Monograph Series vol. 106: Faulting and Magmatism at Mid-Ocean Ridges*, pp. 59–116, American Geophysical Union.

Polster, A., M. Fabian, and H. Villinger (2009), Effective resolution and drift of Paroscientific pressure sensors derived from long-term seafloor measurements, *Geochemistry Geophysics Geosystems*, *10*(8), doi:10.1029/2009GC002532.

Shapiro, S. A., and C. Dinske (2009), Fluid-induced seismicity: Pressure diffusion and hydraulic fracturing, *Geophysical Prospecting*, *57*(2), 301–310.

Shipboard Scientific Party. (1992a), Site Report: Site 857, *In* Davis, E.E., Mottl, M.J., Fisher, A.T., et al., *Proc. of the Ocean Drill. Program, Init. Repts*, *139*, College Station, TX (Ocean Drilling Program), 283–429.

Shipboard Scientific Party. (1992b), Site Report: Site 858, *In* Davis, E.E., Mottl, M.J., Fisher, A.T., et al., *Proc. of the Ocean Drill. Program, Init. Repts*, *139*, College Station, TX (Ocean Drilling Program), 431–569.

Shipboard Scientific Party. (1998a), Middle Valley : Dead Dog Area (Site 1036), *In* Davis, E.E., Mottl, M.J., Fisher, A.T., et al., *Proc. Ocean Drill. Program, Init. Rept*, *169*, College Station, TX (Ocean Drilling Program), 153–203.

Shipboard Scientific Party. (1998b), Middle Valley: Bent Hill Area (Site 1035), *In* Davis, E.E., Mottl, M.J., Fisher, A.T., et al., *Proc. ODP, Init. Rept*, *169*, College Station, TX (Ocean Drilling Program), doi:doi:10.2973/odp.proc.ir.169.103.1998

Sohn, R. A., J. A. Hildebrand, and S. C. Webb (1999), A microearthquake survey of the high-temperature vent fields on the volcanically active East Pacific Rise (9° 50'N), *Journal of Geophysical Research*, *104*(B11), 25367–25377

Stakes, D. S., and J. M. Franklin (1994), Petrology of igneous rocks at Middle Valley, Juan de Fuca Ridge: Major and Trace Element Analyses, *Proc. Ocean Drill. Program Scientific Results*, *139*, 79–102.

Stein, J. S., and A. T. Fisher (2001), Multiple scales of hydrothermal circulation in Middle Valley, northern Juan de Fuca Ridge: Physical constraints and geologic models, *Journal of Geophysical Research*, *106*(B5), 8563–8580.

Turcotte, D. L., and G. Schubert (2002), *Geodynamics*, Cambridge University Press.

Villinger, H. W., M. G. Langseth, H. M. Gröschel-Becker, and A. T. Fisher (1994), Estimating in situ thermal conductivity from log data, *Proc Ocean Drill Program, Scientific Results*, *139*, 545–552.

Van Ark, E. M., R. S. Detrick, J. P. Canales, S. M. Carbotte, A. J. Harding, G. M. Kent, M. R. Nedimovic, W. S. D. Wilcock, J. B. Diebold, and J. M. Babcock (2007), Seismic structure of the Endeavour Segment, Juan de Fuca Ridge: Correlations with seismicity and hydrothermal activity, *Journal of Geophysical Research*, *112*(B02401).

Van Wagoner, N. A., and M. I. Leybourne (1991), Evidence for magma mixing and a heterogeneous mantle on the West Valley segment of the Juan de Fuca Ridge, *Journal of Geophysical Research*, *96*(B10), 16295–16318.

Wang, K., and E. E. Davis (1996), Theory for the propagation of tidally induced pore pressure variations in layered subseafloor formations, *Journal of Geophysical Research*, *101*(B5), 11483–11495, doi:10.1029/96JB00641.

Wheat, C. G., and A. T. Fisher (2007), Seawater recharge along an eastern bounding fault in Middle Valley, northern Juan de Fuca Ridge, *Geophysical Research Letters*, *34*(20), doi:10.1029/2007GL031347.

Zoback, M. D., and H. P. Harjes (1997), Injection-induced earthquakes and crustal stress at 9 km depth at the KTB deep drilling site, Germany, *Journal of Geophysical Research*, *102*(B8), 18477–18491.